NASA TN D-278

TECHNICAL NOTE

D-278

FREE-FLIGHT OBSERVATION OF A SEPARATED TURBULENT FLOW INCLUDING HEAT TRANSFER UP TO MACH 8.5

By Dudley George McConnell

Lewis Research Center
Cleveland, Ohio

NATIONAL AERONAUTICS AND SPACE ADMINISTRATION
WASHINGTON

October 1961

NATIONAL AERONAUTICS AND SPACE ADMINISTRATION

TECHNICAL NOTE D-278

FREE-FLIGHT OBSERVATION OF A SEPARATED TURBULENT FLOW INCLUDING HEAT TRANSFER UP TO MACH 8.5

By Dudley George McConnell

SUMMARY

A turbulent boundary layer separated by a forward-facing step was observed on the cylindrical portion of a hemisphere-cone-cylinder test vehicle. Tip blunting, producing a shear flow, was found to induce higher pressures on the cylindrical portion than were predicted from ballistic tunnel data of unblunted projectiles. An approximate method for predicting this blunt-body pressure distribution was hypothesized. These findings, along with the hypothesis, were substantiated by a wind tunnel test of a similar body. The peak pressure ratios of the separation were smaller in magnitude than flat plate theory predicted because of the effect of the shear flow. The decrement in heating of the separated flow, relative to the corresponding attached flow, was found to compare well with the expected results.

INTRODUCTION

There have been several analytical attempts to determine the nature of turbulent separation, but inherent difficulties have thus far made the problem highly intractable. Therefore, recourse has been made to systematic experimental investigation, which, along with analyses of simplified models, has shed considerable light on this phenomenon. To this end, it was felt that test data obtained in free flight, under conditions of high Mach number and high Reynolds number, would be useful both to theoreticians studying the problem and to designers working in the field.

This study was undertaken at the Lewis Research Center as part of an extensive series of free-flight investigations of boundary-layer transition and heat transfer.

APPARATUS AND INSTRUMENTATION

The test section, with separation collar and boundary-layer tripping device, shown in figure 1, was assembled as follows. A 1/2-inch annulus, 6.00 inches in inside diameter and 0.40 inch wide, was mounted on the cylindrical portion of a 15° cone-cylinder test section. The test section itself was composed of a 1/32-inch-nominal-thickness rolled Inconel cylinder smoothly joined to a 1/16-inch-nominal-thickness rolled nickel conical section, to which was welded a solid-nickel nosepiece having a 7/8-inch-diameter tip.

After installation of the pressure and temperature instrumentation, locations of which are shown in figure 1(a), the test section was polished to a mean roughness height of 1 to 2 microinches, after which the cylindrical portion was vapor-blasted to a roughness height of 55 to 60 microinches. The thermocouples were commutated to record every 0.2 second, and a device was incorporated to record a zero-, half-, and full-scale calibration every 0.2 second. The model instrumentation further consisted of a positive and a negative axial accelerometer, two lateral accelerometers in quadrature, and two static-pressure taps located on the cylindrical portion of the test section. The forward pressure station was located 3 inches aft of the cone-cylinder junction in order to give local static pressure ahead of the interaction; and the after pressure station was located 3 to 4 boundary-layer thicknesses ahead of the separation device, as suggested in reference 1, to measure the peak pressure.

A boundary-layer trip was employed to maintain turbulent flow on the cylindrical portion of the test section. The tripping device consisted of a band of three-dimensional roughness elements of roughness height of 0.030 inch. The design was based on the analysis of roughness effects in reference 2 with boundary-layer calculations based on the method of reference 3. The design presumed that the most unfavorable conditions for inducing turbulence would consist of a laminar boundary layer developing in a reduced Mach number layer because of bluntness effects, as predicted in reference 4. A Reynolds number profile based on distance from the wall was calculated, and a roughness height was then chosen to give a Reynolds number based on roughness height Re_k equal to 900. (Symbols are defined in appendix A.) This number is greater than that suggested in reference 2 by a "factor of safety" of 1.5.

The test vehicle was propelled by a two-stage, solid-propellant rocket combination of a T-64 Recruit first stage and a T-55 second stage. The test section was mounted on the second stage and utilized the motor casing as a telemeter antenna. The two rocket stages were joined by means of a frangible coupling disk, and aerodynamic stability was accomplished by means of cruciform fins on the first stage and a 10° flared skirt on the main stage. The complete assembly is shown in figure 1(c).

EXPERIMENT

The flight test vehicle was launched over the NASA tracking range at Wallops Island, Virginia, from a B57 aircraft at an altitude of approximately 45,000 feet. The rocket stages were ignited by separate time-delay squibs which were energized upon the vehicle's release from the parent craft. Tracking was accomplished by radar, and ambient conditions were obtained from a survey by a Rawinsonde balloon launched just prior to vehicle release. The instrument measurements were telemetered to the tracking station and recorded there. Because of an instrumentation difficulty of unknown origin, the thermocouple channel recorded only intermittently after 4.0 seconds after first-stage ignition; the rest of the instruments performed satisfactorily.

A tunnel test was also performed on a similar body in order to verify certain of the following results.

RESULTS AND DISCUSSION

A flight trajectory was obtained by matching an integration of the axial accelerometer recordings with the radar position at first-stage ignition. The flight trajectory, Mach number, and free-stream unit Reynolds number histories thereby obtained are shown in figures 2, 3, and 4, respectively. Investigations of the lateral accelerometer recordings showed that no appreciable angle of attack (less than $1/2^{\circ}$) was experienced by the missile until about 11 seconds after first-stage ignition, when an angle of attack of 2° in the yaw plane developed. From that point onward, the vehicle experienced small, aperiodic disturbances of that magnitude.

Attached-Flow Pressure Measurements and Bluntness Effect Hypothesis

A comparison of the measured static pressure at the forward pressure station $p_{c,1}$ with that predicted to have occurred there (for an unblunted cone) is shown in figure 5. The predictions were based on the ambient pressure p_{∞} and ballistic tunnel data reported in reference 5. This comparison shows a large discrepancy between measured and predicted values, the predicted values being much smaller. At first it was felt that the increased pressures might have been due to detachment at the cone-cylinder junction, aided by the tripping device, and subsequent reattachment in the vicinity of the forward pressure station. However, tunnel tests of higher angle cones failed to show this detachment, and the trip was much smaller than the disturbance height necessary to cause detachment.

An application of the data of reference 6 to this vehicle showed the low Mach number layer, due to bluntness effects, to have been of approximately the same height as the boundary layer on the after portion of the cone (see fig. 6). This suggested as a working hypothesis that the expansion at the cone-cylinder junction took place at the reduced Mach number. Furthermore, an approximate value for the controlling cone Mach number was obtained by matching the cone and cylinder pressures with a Prandtl-Meyer expansion. The matching showed this cone Mach number to have been very close (i.e., within 10 percent) to the Mach number predicted for the edge of the low Mach number layer. Figure 5 shows that the measured pressures are somewhat smaller than those predicted by this lower Mach number expansion, but also that the patterns of variation are markedly similar. This variational pattern is quite dissimilar to the pattern predicted by reference 5. The computational procedure used in obtaining the blunted pressure distribution is outlined in appendix B.

Substantiation of Bluntness Hypothesis

For experimental substantiation of the bluntness hypothesis, a tunnel program was initiated. The results of that program are shown in figure 7, which presents the static-pressure distribution on a blunted and unblunted $15^{\circ}55'$ cone-cylinder in a Mach 4.95 stream at zero incidence. The pressures on the cone are compared with the potential flow solution and the modified Newtonian approximation (modified by adjusting the maximum pressure coefficient to give the proper value for the nose pressure). The cylinder pressures are compared with those predicted by reference 5. The fact that the pressures on the cone fall below the potential flow solution can be attributed to overexpansion at the hemisphere-cone junction. The essential point demonstrated is the following: Even though the pressures on the blunted cone are low, the cylinder pressures on the blunted model are greater than those on the unblunted model and are some 20 percent greater than the predicted distribution. Still further qualitative substantiation of this hypothesis was reported by Whitfield and Potter in reference 7. They were able to correlate base pressures behind blunted cones by assuming that an expansion at a hypothetical cone-cylinder junction took place at a mean Mach number between the blunted and the sharp-tipped values. All this evidence seemed to substantiate, at least qualitatively, the hypothesis of a Prandtl-Meyer expansion at some reduced Mach number. A consideration of the heat-transfer data is in order before further discussion of the pressure data.

Attached Flow Heat-Transfer Measurements

Heat-transfer coefficients were obtained from the data by the relation

$$h = \frac{\rho_w C_w \tau_w (dT_w/dt)}{T_{aw} - T_w}$$

The recovery factors used in finding the adiabatic wall temperatures T_{aw} were $r = (Pr)^{1/2}$ and $r = (Pr)^{1/3}$ for laminar and turbulent flows, respectively. Stanton numbers were obtained from the definition $St = h/\rho_e u_e c_{p,e}$ and were compared with the relevant theory of Van Driest (ref. 8), and the Nusselt numbers were compared with the theory of Reshotko (ref. 9). These comparisons are presented in figures 8 to 12. The primary reason for the temperature measurements was to ascertain whether or not the tripping device was successful in maintaining turbulent flow on the cylindrical section. To this end, the data show that in terms of heat transfer the flow was turbulent over the whole period for which reliable temperature data were obtained (i.e., up to 4.0 sec). However, additional information concerning the flow over this blunt body was also obtained. This information is especially vital to a discussion of the data pertaining to the separated region.

Emergence of the boundary layer from the low Mach number layer - cylindrical section. - In the vicinity of 2.5 seconds and shortly thereafter, the Stanton numbers on the cylindrical section increased very rapidly with time. Also, the Stanton numbers on the cone showed this same increase over their previous values. Attempts were made to rationalize the cone data by attributing the large changes in Stanton number to a slow (in time) transition to turbulent flow. This position was deemed untenable because: first, the deviation of the cylinder from theory could not be accounted for on this basis; and, second, plots of Stanton number against Reynolds number Re_x, were not at all similar in character to generally accepted transitional patterns. Therefore another approach was sought. At this time the work of Kendall (ref. 6) came to hand. This report shed considerable light on the nature of the low Mach number layer.

Moeckel (ref. 4) defines the edge of the low Mach number layer as being the streamline which passes through the sonic point of the bow wave. That this is an arbitrary definition is shown later in reference 4 in the plots of the Mach number profile. In short, the Mach number does not reach the free-stream value for several low Mach number layer thicknesses. The pertinent contribution of Kendall's data is to show how the sonic point of the bow wave approaches the vertex as the flight Mach number increases. This has the net effect of demonstrating how the shear layer thickness at a particular axial location varies with Mach number (and in this case time). On the other hand, the analysis of reference 3 shows that the thickness of the laminar boundary layer varies inversely with unit Reynolds number and increases with increasing edge Mach number. Initially, as time increases, the unit Reynolds number decreases slightly and the reduced Mach number increases. At a particular axial location on the cone then, the reduced Mach number layer thickness decreases, and the boundary-layer thickness increases with Mach number for this trajectory. The calculated variations of reduced Mach number layer and boundary-layer

thicknesses are presented in figure 6. Since the boundary-layer thickness exceeds the reduced Mach number layer thickness, a consideration of the heat-transfer data in terms of "sharp-tip" conditions appeared to be in order. The Stanton number histories are presented in figures 10 and 11 in terms of sharp tip conditions. In the vicinity of 3.5 seconds and thereafter the data compared reasonably well with theory based on sharp-tip edge conditions. Before this time however (between 2.5 and 3.5 sec) the data did not compare with either method of prediction. This is no less than should be expected because there is no adequate means of determining what the conditions at the edge of the boundary layer might be.

Emergence of boundary layer from low Mach number layer - conical section. - The results of the heat-transfer measurements made on the conical portion are presented in figure 12 in terms of a heat-transfer parameter $Nu/\sqrt{Re_w}$. From 1.0 to 3.0 seconds the heat transfer at the four forward stations compares reasonably well with theory; whereas the heating at the three rearward stations tends to be low initially and compares well only between 2.0 and 3.0 seconds. After 3.0 seconds both the forward and rearward stations increase rapidly. The divergence from theory here is of the same order as that which occurred on the cylinder. However, comparisons with the sharp tip theoretical Stanton numbers did not show the same agreement as obtained on the cylindrical section. This was due to the fact, demonstrated in figure 6, that the boundary layer on the cone was not large enough to dominate the shear layer as it did on the cylindrical portion. Hence, the emergence as determined from the heating was not as clearly defined.

Separated flow. - In light of the foregoing, the data concerning the separated region will be discussed. The peak pressures measured in the separated region $p_{c,2}$ are presented in figure 13; and the ratios of $p_{c,2}$ to p_∞ and $p_{c,2}$ to p_l, the local pressure ahead of separation, are presented in figures 14 and 15, respectively. Now for separation data obtained in wind tunnel tests the assumption is made that the boundary layer ahead of the separation develops in a uniform flow. In the present test, however, the boundary layer develops in a region of shear. Consequently, the boundary-layer velocity profile is less "full" than that profile that would exist in a corresponding development in a uniform flow (with the same edge conditions); and therefore the form factor is greater. Hence, according to the analysis of reference 10, for the same Mach number at the edge of the boundary layer one would expect lower peak pressure ratios than those obtained for the shock-induced breakaway of a boundary layer developing in a uniform flow. The comparison of the data with the theory of reference 10 bears out this conclusion.

The heat-transfer coefficients, obtained from measurements made in the separated region, are compared with those predicted to occur on a cone frustum replacing the dead air region. This comparison is presented

in figure 16. The cone-frustum heating was calculated using fluid properties calculated after the method of Eckert (ref. 11), the measured peak pressure, the length of turbulent run to thermocouple station 12, and the Mach number and static temperature existing behind the normal shock. The measured heat-transfer coefficients are 40 to 50 percent less than the cone-frustum values. This decrement is in reasonable agreement with the data of reference 12. The measured heat-transfer rates at thermocouple stations 10 and 12 are presented in figure 16(b). Reference to figure 13 shows "dips" in the measured peak pressure at Mach numbers 6.28 (between stages) and 8.22 (just after peak Mach number). These breaks are also shown in the rates of heat transfer. At these times the vehicle had just passed through zero acceleration; hence, the boundary layer was not even quasi-steady. As stated earlier, the angles of attack experienced by the missile at these times were small. Therefore, the abrupt changes in peak pressure and heat-transfer coefficient just before second-stage ignition and just after peak Mach number were due to body forces, rendering the region of separation nonsteady at these times.

CONCLUSIONS

This study was initiated in order to obtain free-flight data on separated turbulent flows. Because of the boundary-layer development in a shear flow prior to separation, the peak pressure ratios at separation were lower than those calculated from flat plate theory. Therefore these data on peak pressure ratios are not to be compared with other data where the flow external to the boundary layer was uniform (e.g., ref. 13). The heat-transfer data, however, do reproduce the roughly predictable decrement in heating, 40 to 50 percent, relative to the corresponding attached flow. It was also found that the nose bluntness, by producing the shear flow, modified the inviscid static-pressure distribution on the cylindrical afterbody of the test vehicle.

Lewis Research Center
National Aeronautics and Space Administration
Cleveland, Ohio, January 23, 1961

APPENDIX A

SYMBOLS

C	heat capacity
c_p	specific heat at constant pressure
h	heat-transfer coefficient
M	Mach number
Nu	Nusselt number
P	total pressure
Pr	Prandtl number, ν/α
p	static pressure
R	nose radius
Re	Reynolds number, ux/ν
Re_k	critical Reynolds number based on roughness height
Re_x	Reynolds number based on length of boundary run
r	recovery factor
St	Stanton number
T	temperature
t	time
u	velocity
x	axial distance, ft
α	thermal diffusivity
γ	ratio of specific heats
ν	kinematic viscosity
ρ	density

τ wall thickness

Subscripts:

aw adiabatic wall

c cylinder conditions

e edge of boundary layer

l local

n blunted value

s based on step height

w wall

1 forward pressure station

2 after pressure station

∞ free stream

APPENDIX B

CALCULATION OF BLUNTNESS EFFECT APPROXIMATION

The approximation assumes that a Prandtl-Meyer expansion at the reduced Mach number takes place at the cone-cylinder junction and that this expansion, subject to recompression along the afterbody, determines the afterbody pressure distribution. It is necessary to know the local Mach number and static pressure on the cone. The static pressure on the cone p_c can be found from conical flow charts (e.g., ref. 14) given free-stream Mach number M_∞, ambient pressure p_∞, and cone half-angle θ. The total pressure on the cone P_c can be found from the Rayleigh pitot-tube formula:

$$P_c = \frac{p_\infty \left(\frac{\gamma + 1}{2} M_\infty^2 \right)^{\frac{\gamma}{\gamma - 1}}}{\left(\frac{2\gamma}{\gamma + 1} M_\infty^2 - \frac{\gamma - 1}{\gamma + 1} \right)^{\frac{1}{\gamma - 1}}}$$

where γ is the ratio of specific heats for air. Then the local Mach number is obtained from the ratio of total to static pressure according to the relation

$$\frac{P_c}{p_c} = \left(1 + \frac{\gamma - 1}{2} M_{e,n}^2 \right)^{\frac{\gamma}{\gamma - 1}}$$

A two-term Busemann series then yields the static pressure after expansion at the cone-cylinder junction p_{ej} accordingly as

$$\frac{p_{ej}}{p_c} = 1 + \frac{\gamma}{2} M_{e,n}^2 \left\{ \frac{-2\theta}{\sqrt{M_{e,n}^2 - 1}} + \frac{\left[(M_{e,n}^2 - 2)^2 + \gamma M_{e,n}^4 \right] \theta^2}{2(M_{e,n}^2 - 1)^2} \right\}$$

where the cone half-angle θ must be expressed in radians.

Finally, the ballistic tunnel data of reference 5 were used to determine the recompression on the afterbody.

REFERENCES

1. Kepler, C. E., and Bogdonoff, S. M.: Interaction of a Turbulent Boundary Layer with a Step at M = 3. Rep. 238, Dept. Aero. Eng., Princeton Univ., Sept. 1, 1953. (Contract N6-onr-270.)

2. Braslow, Albert L., and Knox, Eugene C.: Simplified Method for Determination of Critical Height of Distributed Roughness Particles for Boundary-Layer Transition at Mach Numbers from 0 to 5. NACA TN 4363, 1958.

3. Low, George M.: The Compressible Laminar Boundary Layer with Heat Transfer and Small Pressure Gradient. NACA TN 3028, 1953.

4. Moeckel, W. E.: Some Effects of Bluntness on Boundary-Layer Transition and Heat Transfer at Supersonic Speeds. NACA Rep. 1312, 1957. (Supersedes NACA TN 3653.)

5. Clippinger, R. F., Giese, J. H., and Carter, W. C.: Tables of Supersonic Flows About Cone Cylinders. Pt. I. Surface Data. Rep. No. 729, Ballistic Res. Labs., Aberdeen Proving Ground (Md.), July 1950.

6. Kendall, J. M.: Experiments on Supersonic Blunt-Body Flows. Prog. Rep. 20-372, Jet. Prop. Lab., Feb. 27, 1959.

7. Whitfield, J. D., and Potter, J. L.: On Base Pressures at High Reynolds Numbers and Hypersonic Mach Numbers. AEDC-TN-60-61, Mar. 1960.

8. Lee, Dorothy B., and Faget, Maxime A.: Charts Adapted from Van Driest's Turbulent Flat-Plate Theory for Determining Values of Turbulent Aerodynamic Friction and Heat-Transfer Coefficients. NACA TN 3811, 1956.

9. Reshotko, Eli: Simplified Method for Estimating Compressible Laminar Heat Transfer with Pressure Gradient. NACA TN 3888, 1956.

10. Reshotko, Eli, and Tucker, Maurice: Effect of a Discontinuity on Turbulent Boundary-Layer-Thickness Parameters with Application to Shock-Induced Separation. NACA TN 3454, 1955.

11. Eckert, E. R. G.: Engineering Relations for Friction and Heat Transfer to Surfaces in High Velocity Flow. Jour. Aero. Sci., vol. 22, no. 8, Aug. 1955, pp. 585-587.

12. Larson, H. K.: Heat Transfer in Separated Flow. Jour. Aero/Space Sci., vol. 26, no. 11, Nov. 1959, pp. 731-738.

13. Chapman, Dean R., Kuehn, Donald M., and Larson, Howard K.: Investigation of Separated Flows in Supersonic and Subsonic Streams With Emphasis on the Effect of Transition. NACA Rep. 1356, 1958. (Supersedes NACA TN 3869.)

14. Ames Research Staff: Equations, Tables, and Charts for Compressible Flow. NACA Rep. 1135, 1953. (Supersedes NACA TN 1428.)

Instrumentation locations			
Thermocouple station			
Designation	Axial distance, in.	Skin material	Local skin thickness, in.
1	7.00	Nickel	0.0680
2	9.44		.0695
3	11.88		.0700
4	14.32		.0680
5	16.76		.0700
6	19.20		.0700
7	19.20		.0610
8	21.44	Inconel	.0340
9	24.16		.0340
10	26.88		.0335
11	29.60		.0335
12	32.32		.0335

Static-pressure taps		
Designation	Axial distance, in.	Comments
$p_{c,1}$	22.88	To imply free-stream value
$p_{c,2}$	32.60	To give peak pressure

Instrumentation	Range
Thermocouples	400° to 1600° R
Pressure taps	2 to 15 lb/sq in. abs
Positive accelerometer	0 to 160 g's
Negative accelerometer	+5 to -40 g's
Lateral accelerometer	-10 to +10 g's

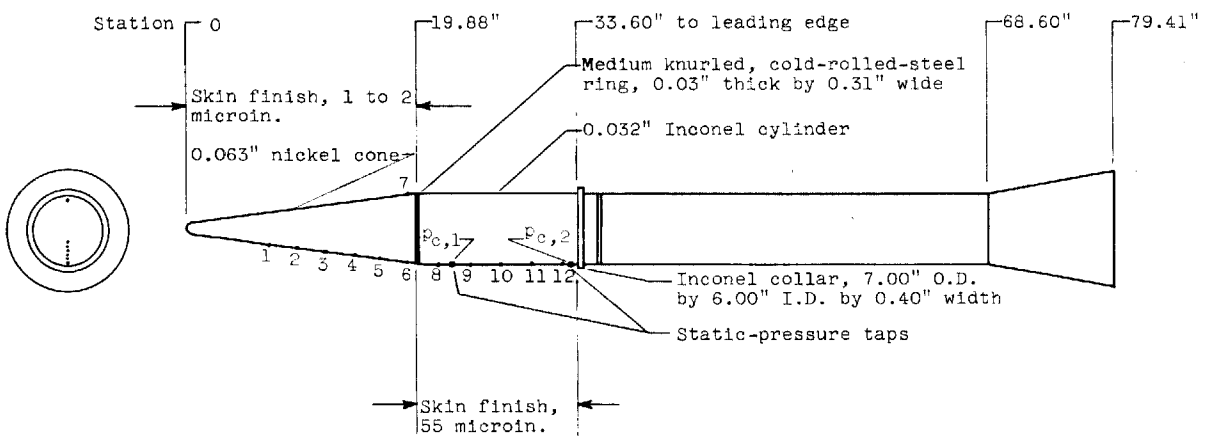

(a) Main stage and test section with instrumentation.

Figure 1. - Test section.

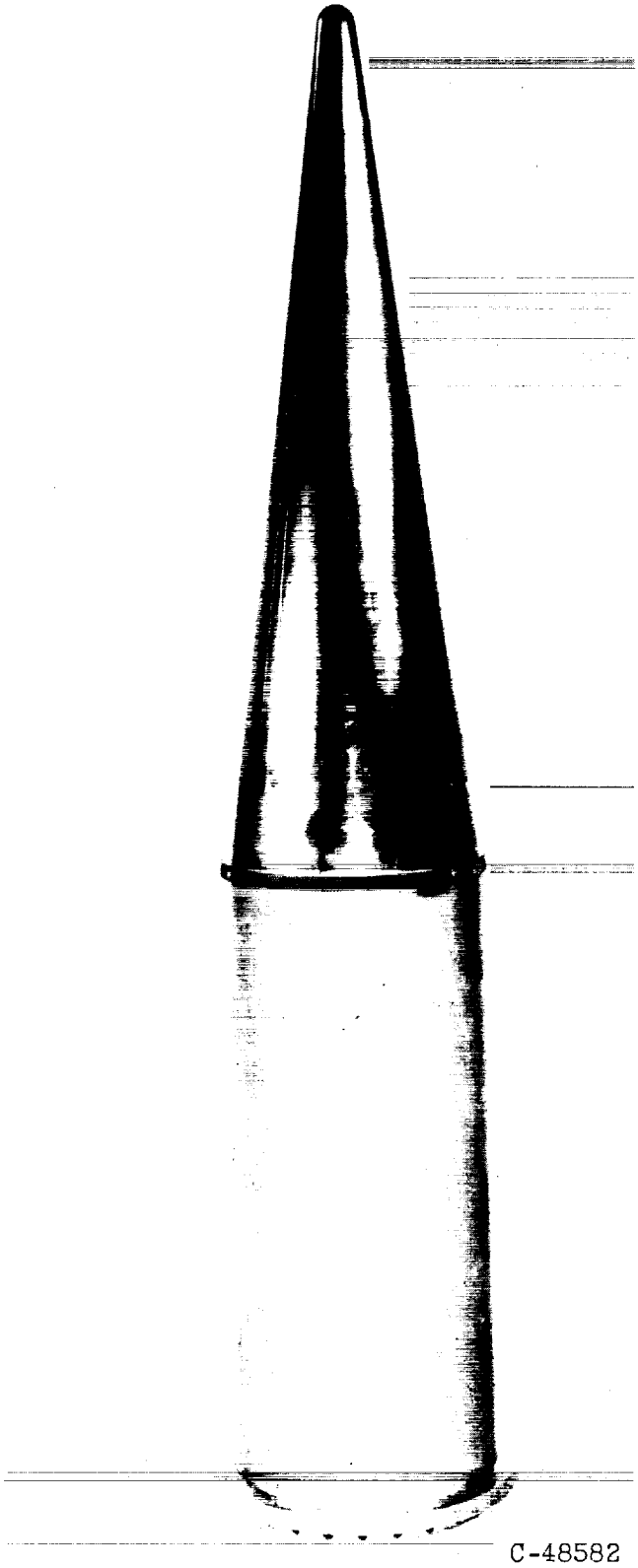

(b) Detail.

Figure 1. - Continued. Test section.

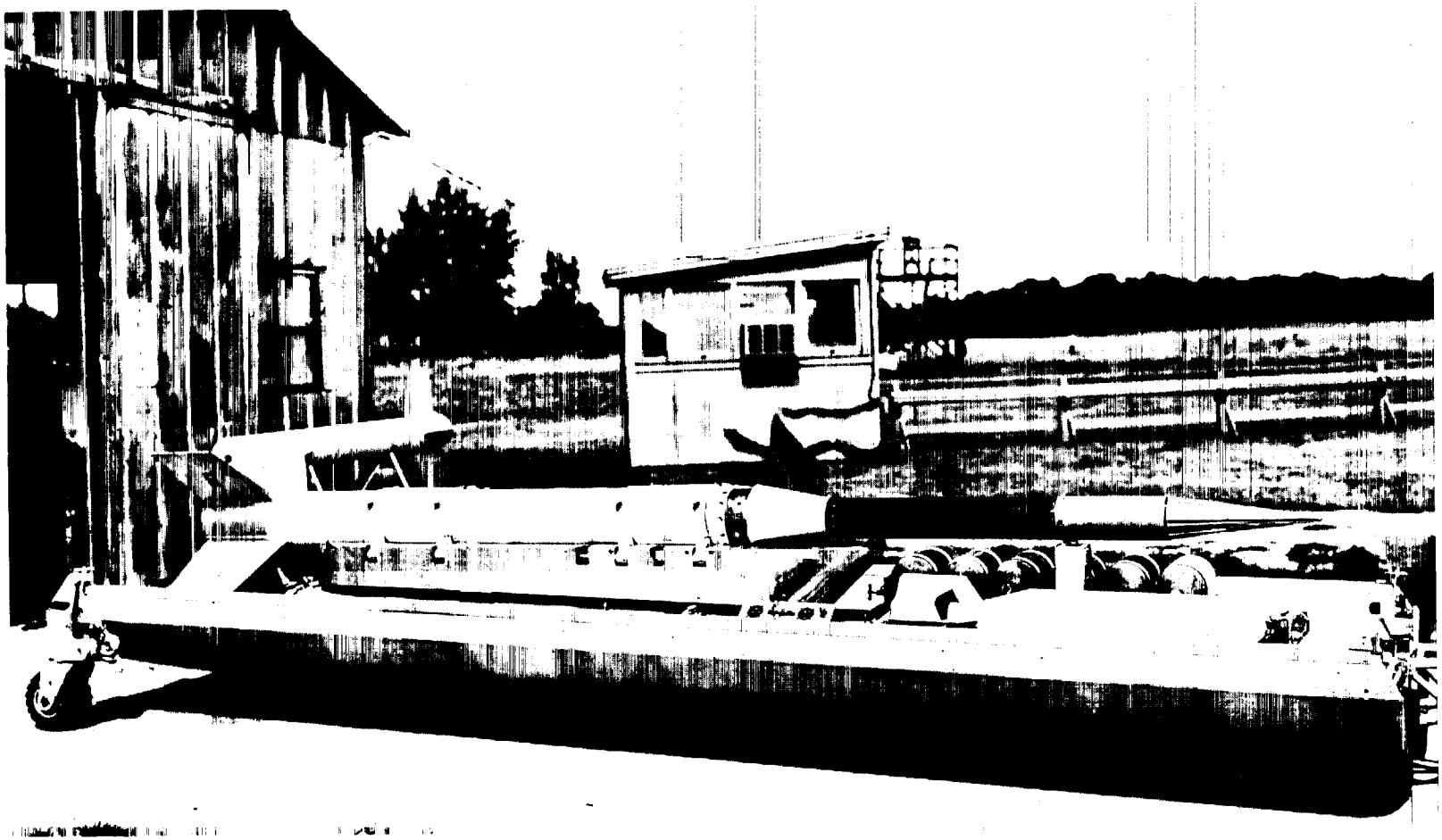

C-48665

(c) Complete test vehicle before takeoff.

Figure 1. - Concluded. Test section.

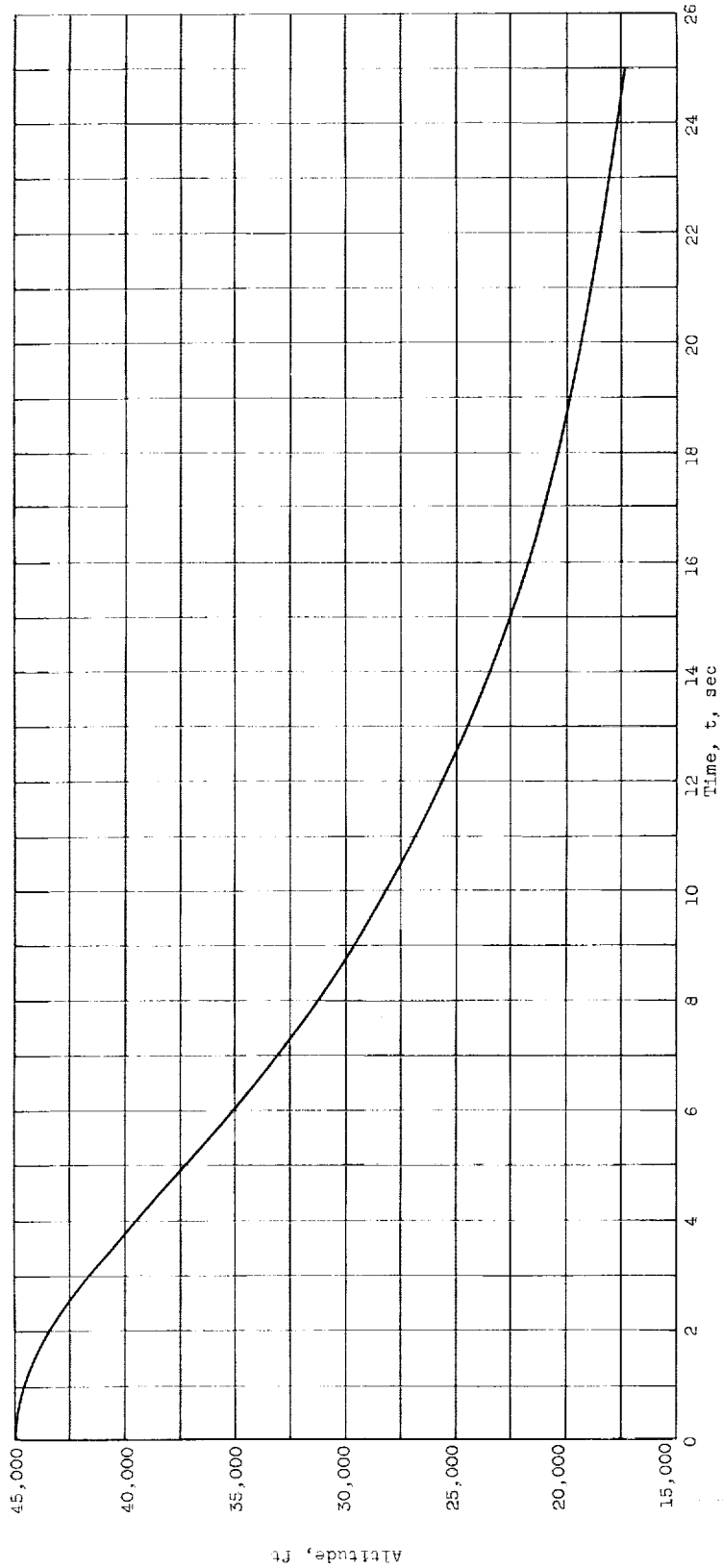

Figure 2. - Flight trajectory.

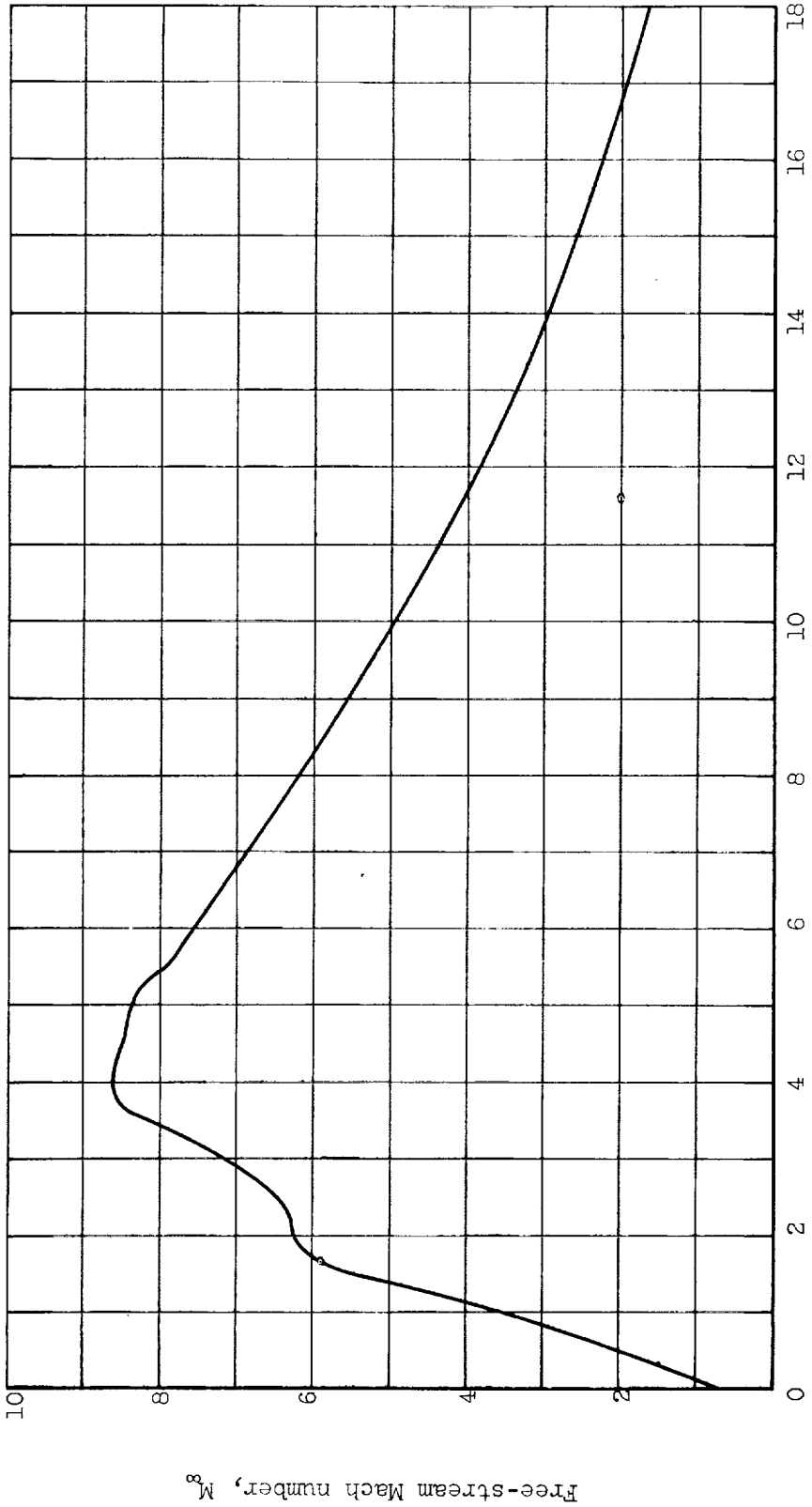

Figure 3. - Mach number history.

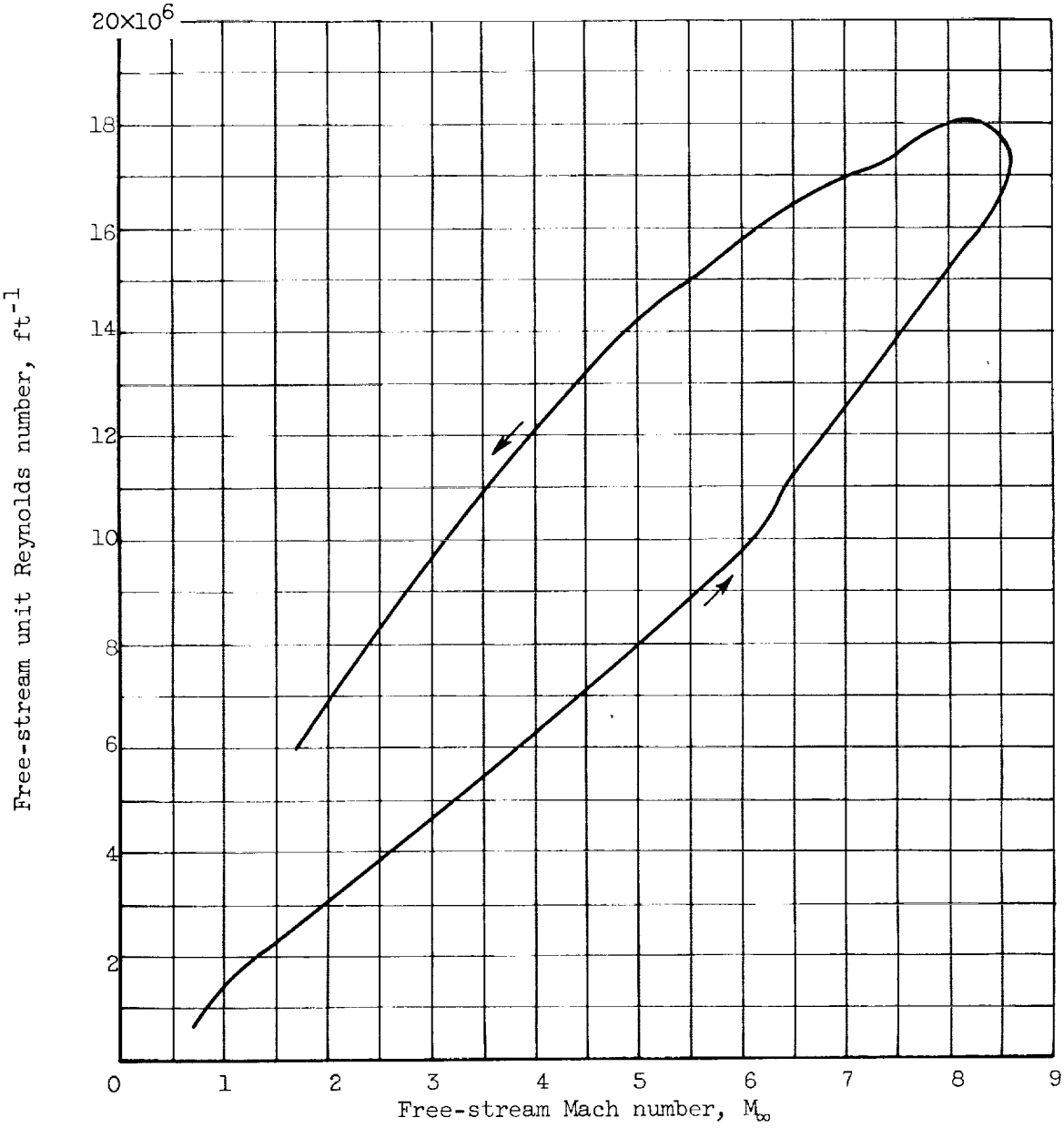

Figure 4. - Flight unit Reynolds number history.

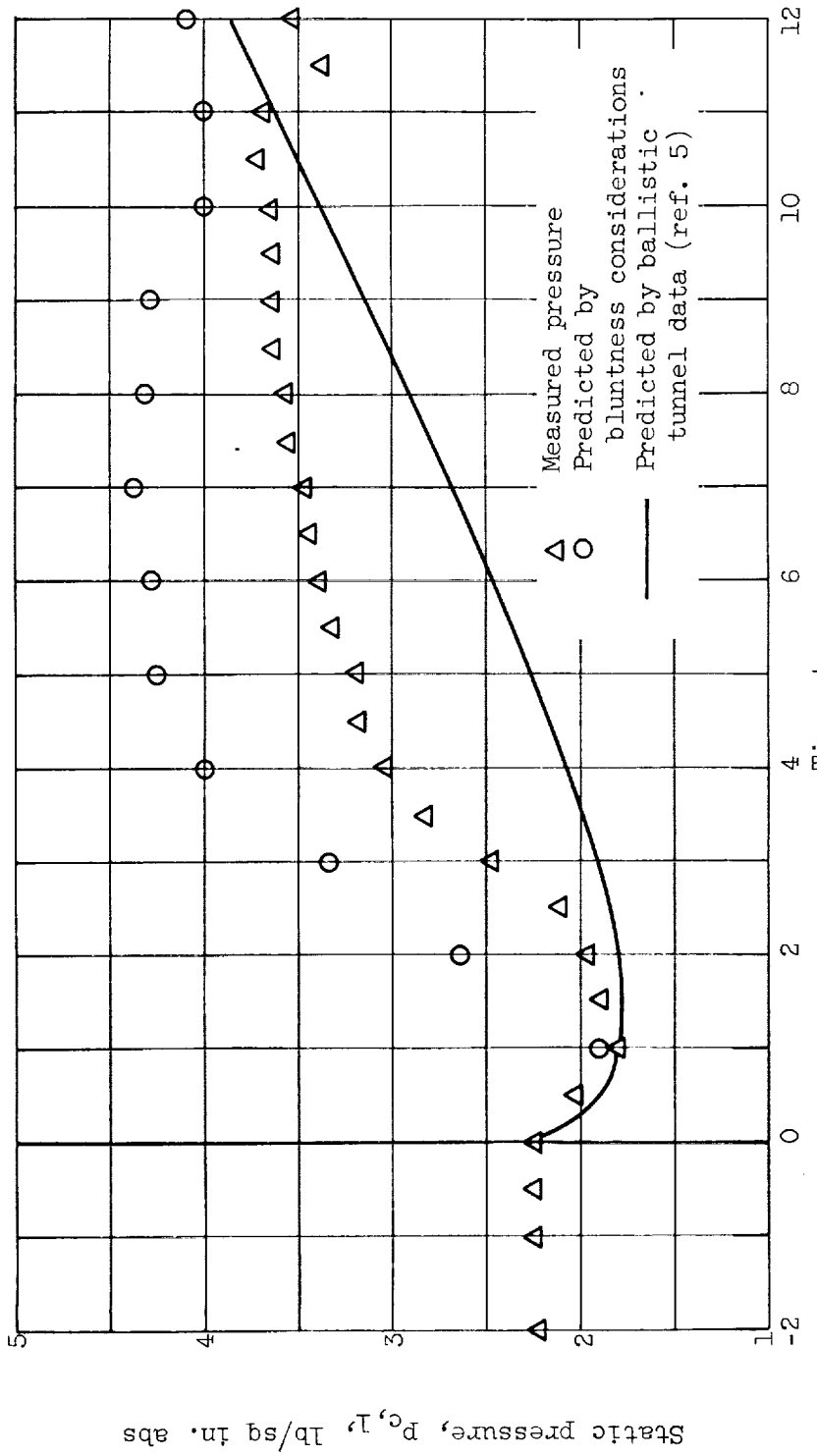

Figure 5. - Comparison of measured and predicted static pressures at forward pressure station.

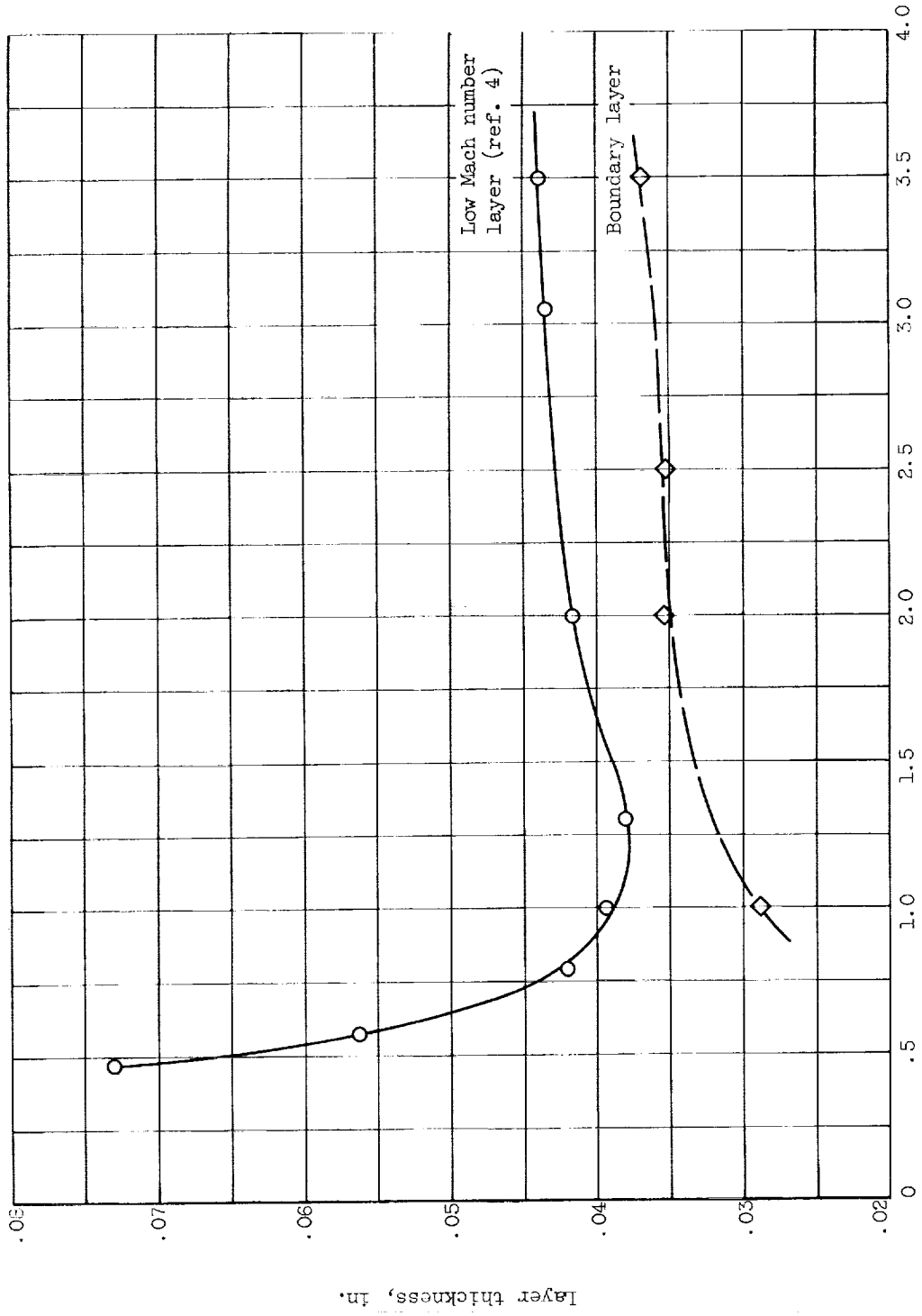

(a) Thermocouple station 4.

Figure 6. - Comparison of boundary layer and shock layer thickness.

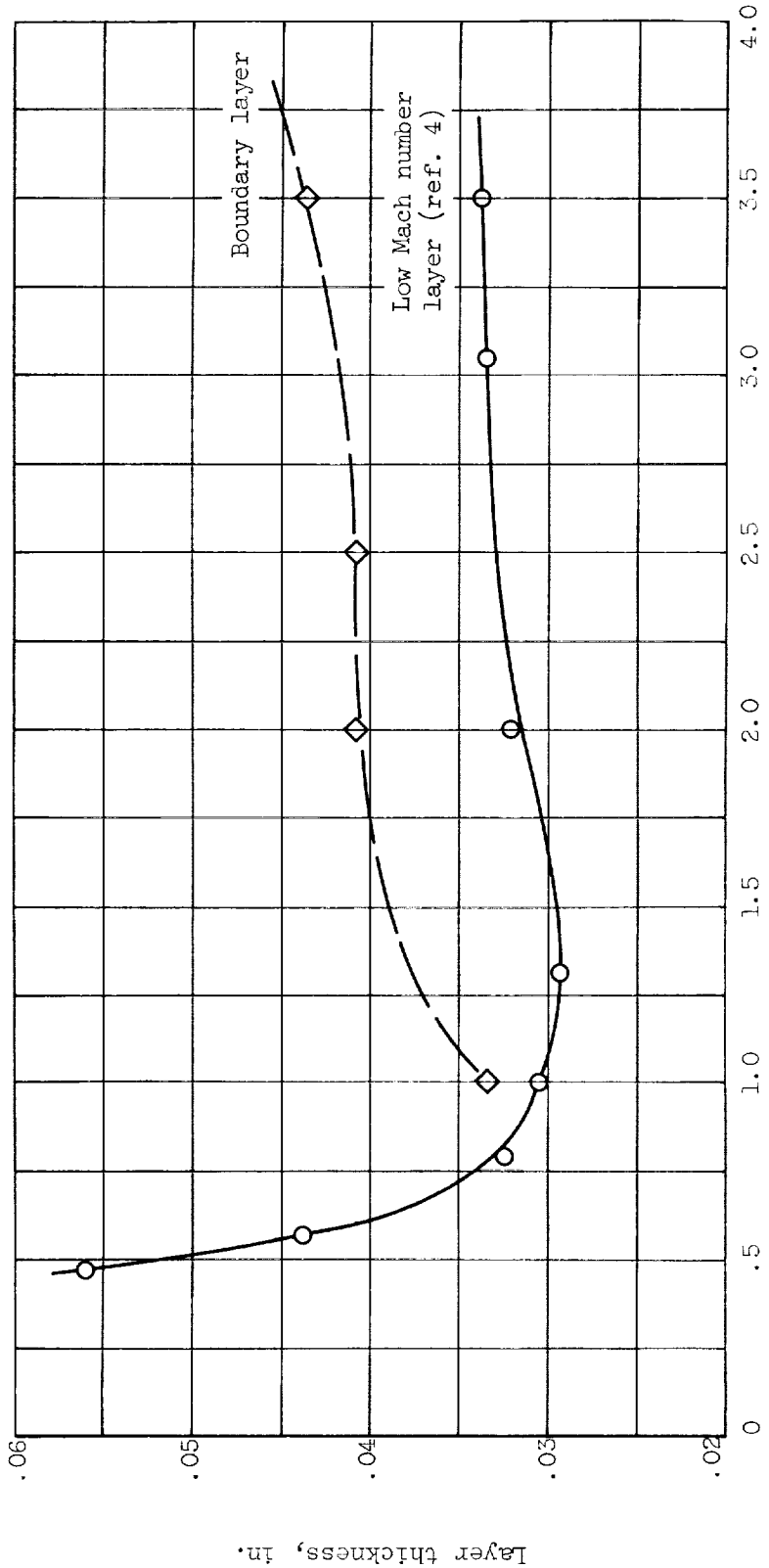

(b) Thermocouple station 6.

Figure 6. - Continued. Comparison of boundary layer and shock layer thickness.

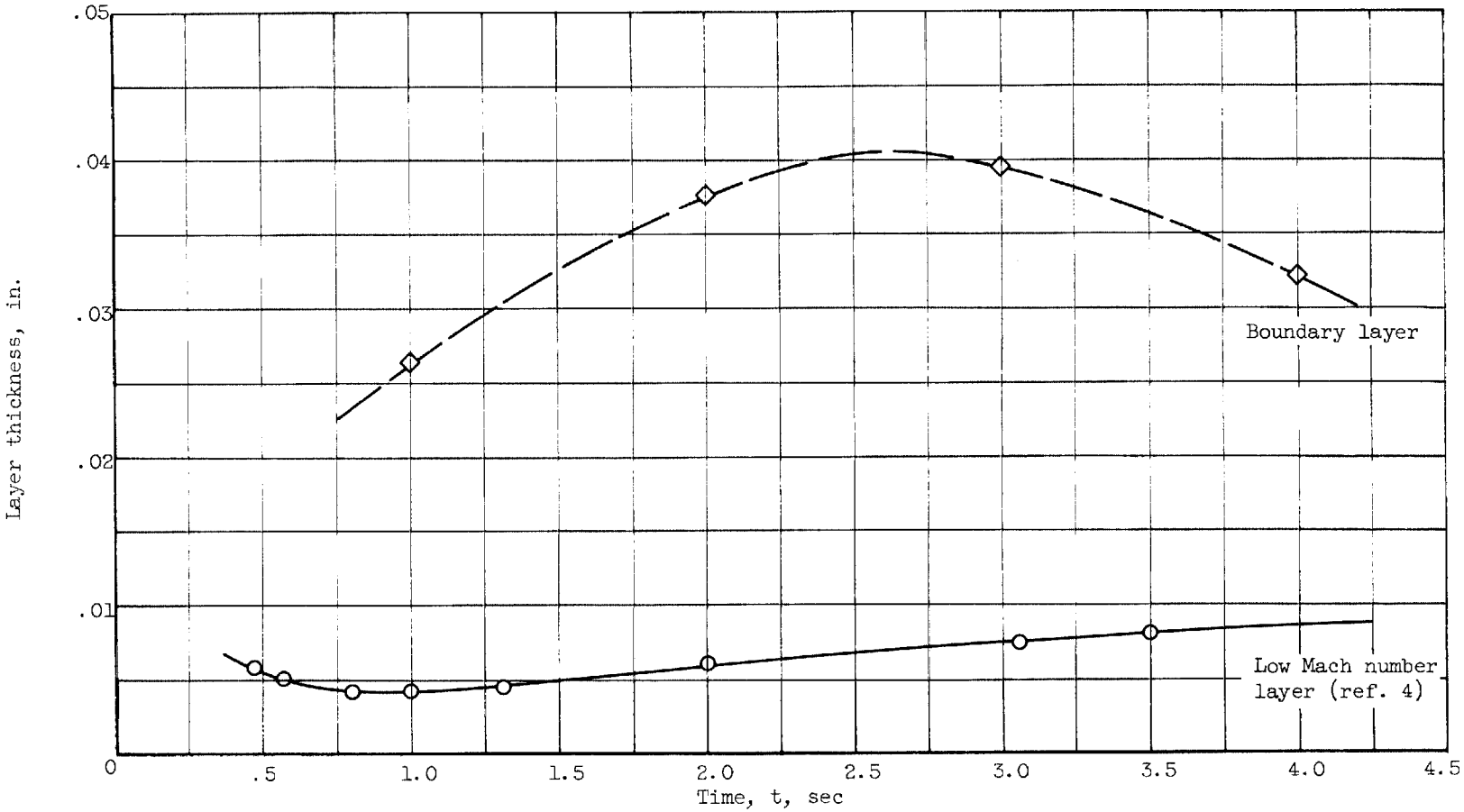

(c) Thermocouple station 10.

Figure 6. - Concluded. Comparison of boundary layer and shock layer thickness.

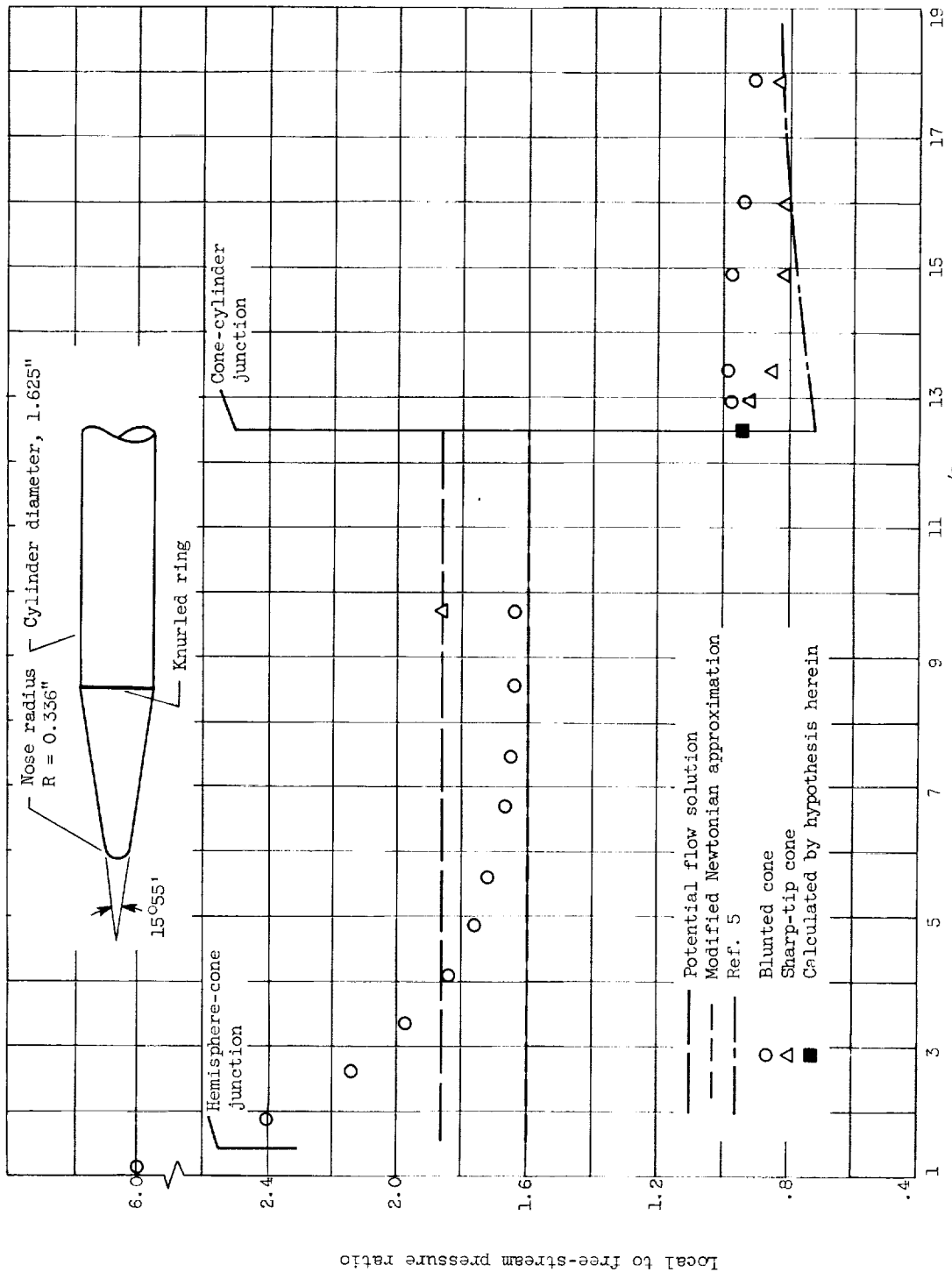

Figure 7. - Pressure distribution on a cone cylinder. Tunnel test free-stream Mach number, 4.95.

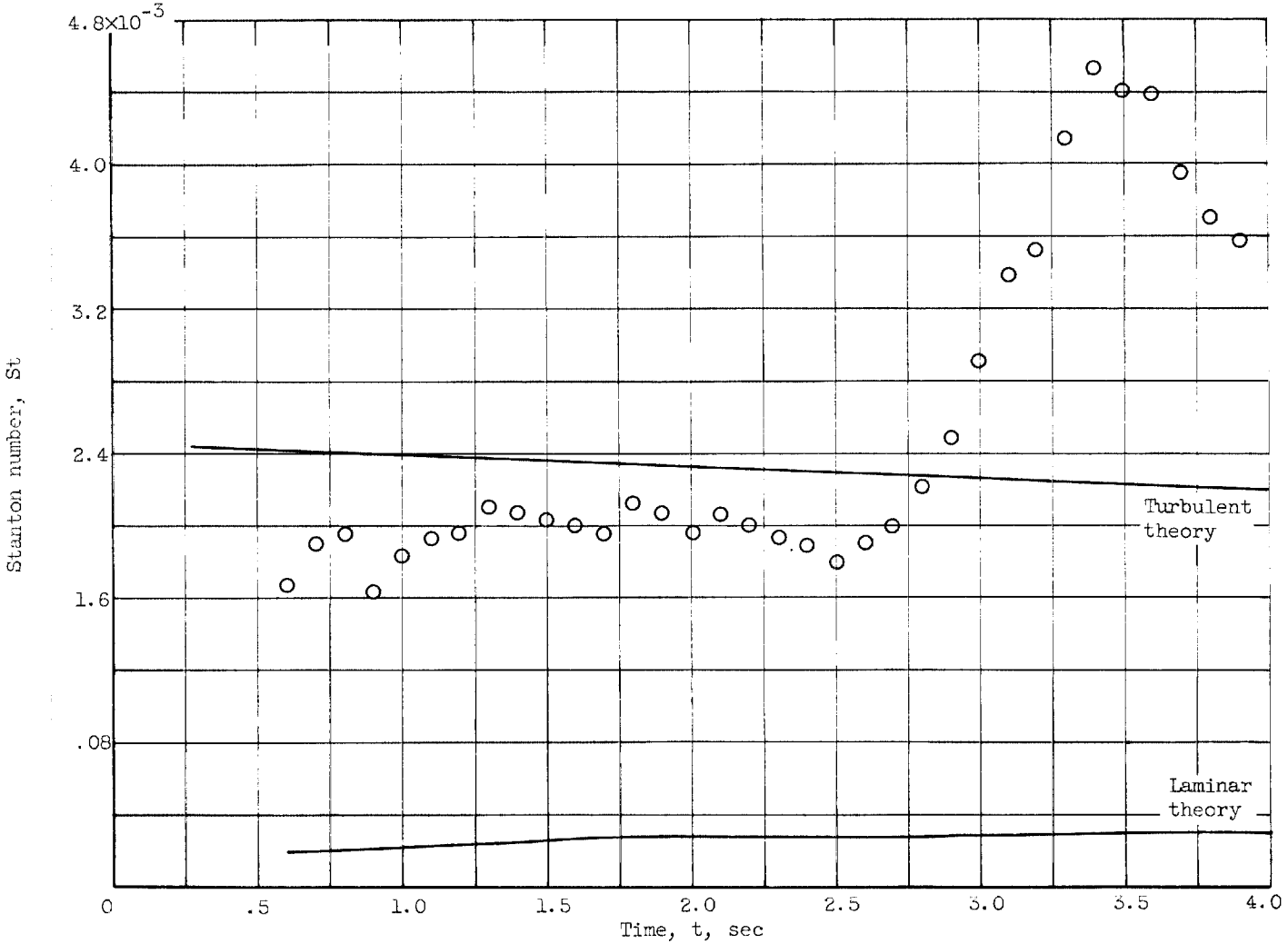

(a) Thermocouple station 8.

Figure 8. - Stanton number histories. Blunt conditions; cylinder stations.

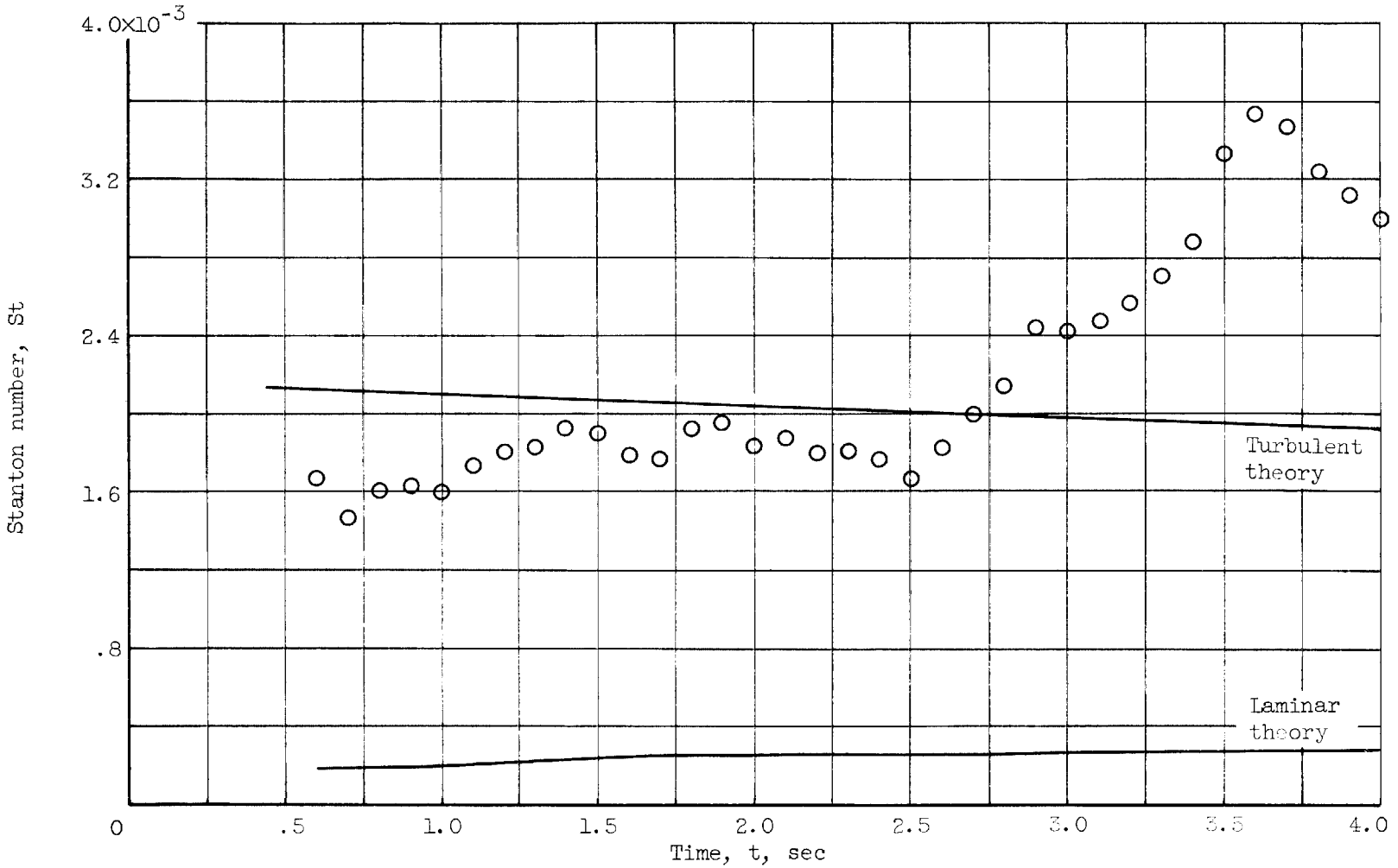

(b) Thermocouple station 9.

Figure 8. - Continued. Stanton number histories. Blunt conditions; cylinder stations.

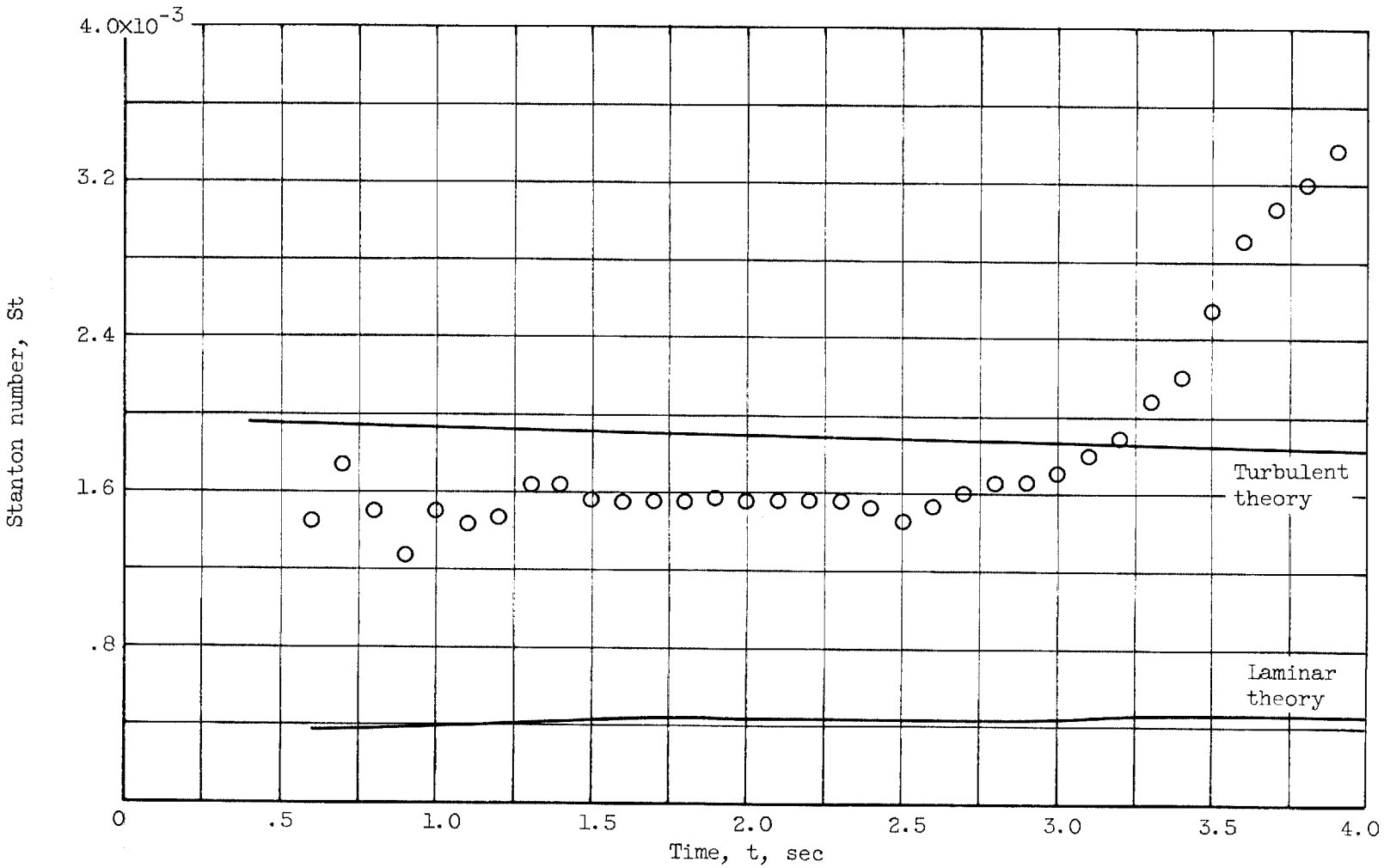

(c) Thermocouple station 10.

Figure 8. - Continued. Stanton number histories. Blunt conditions; cylinder stations.

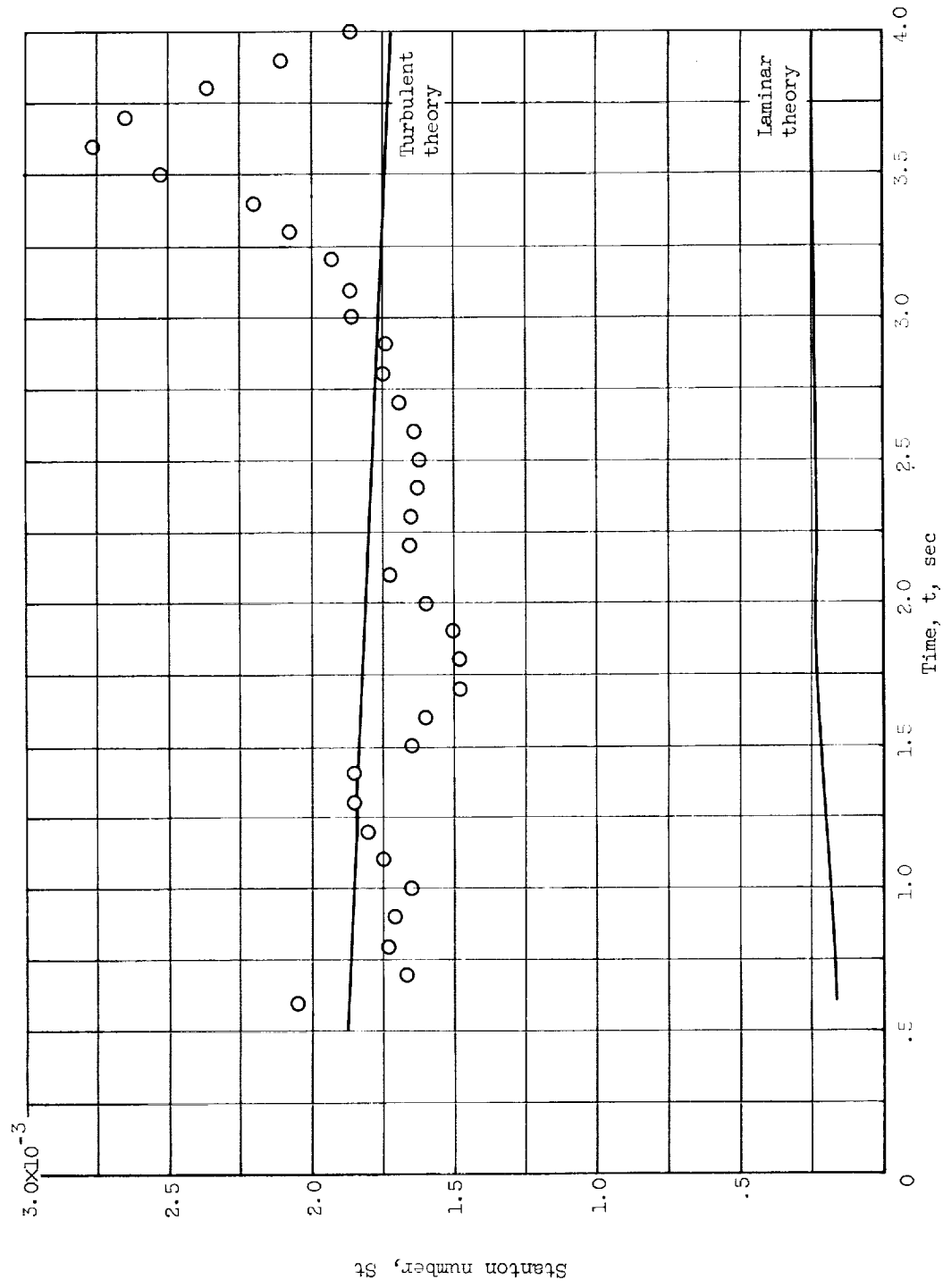

(d) Thermocouple station 11.

Figure 8. - Concluded. Stanton number histories. Blunt conditions; cylinder stations.

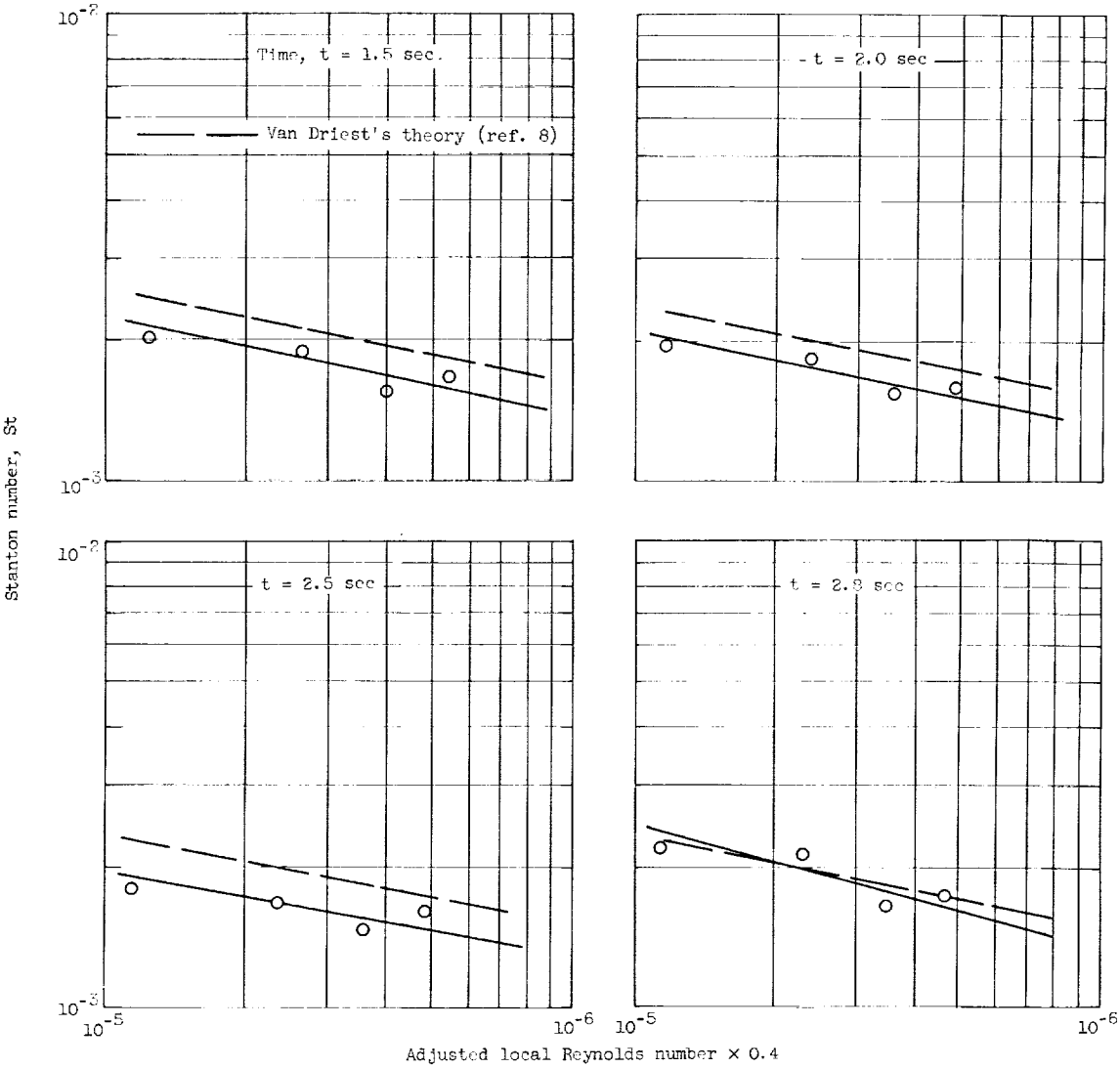

Figure 9. - Stanton number plotted against adjusted local Reynolds number. Blunt conditions; cylinder stations.

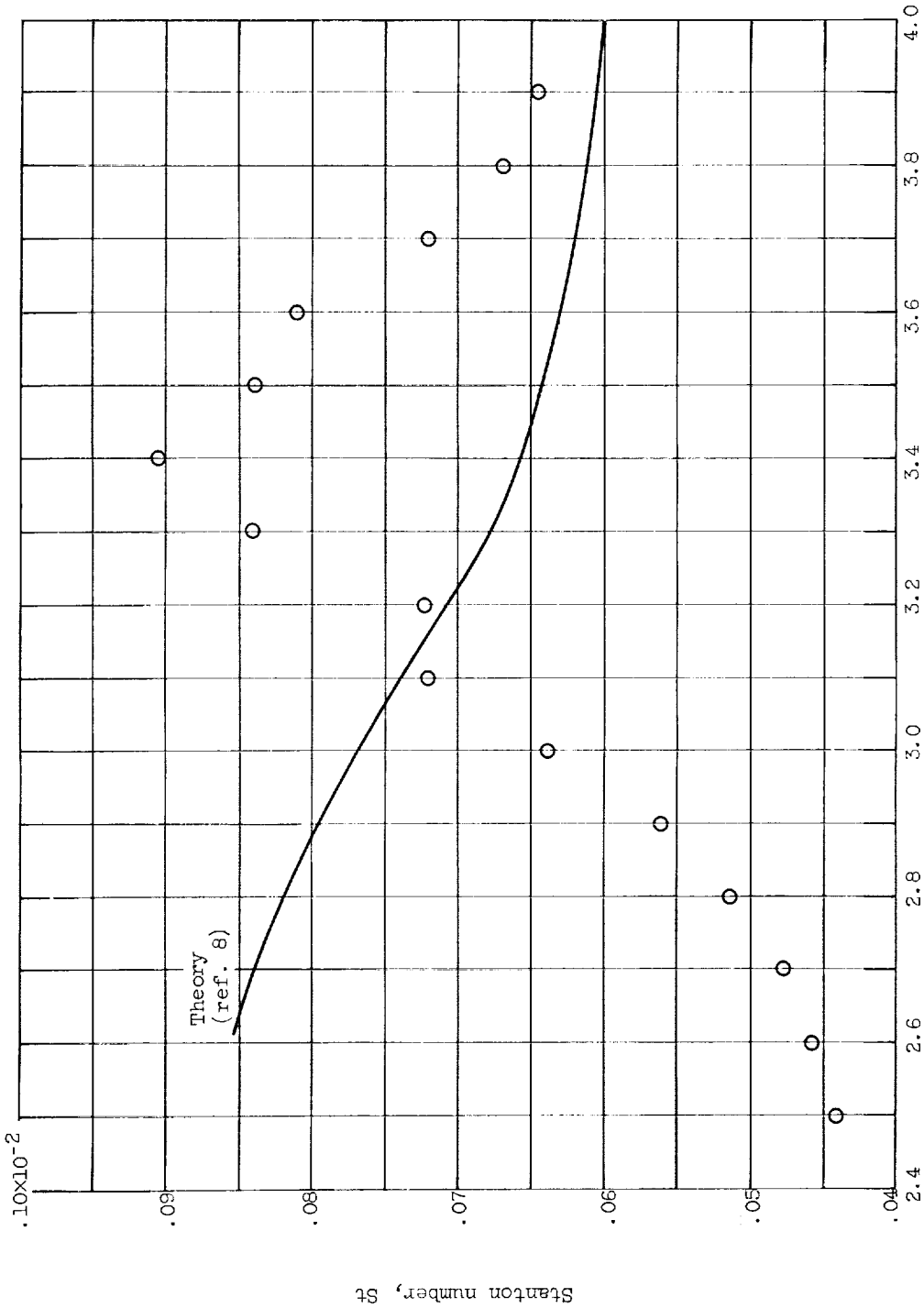

(a) Thermocouple station 8.

Figure 10. - Stanton number histories. Sharp tip conditions; cylinder stations.

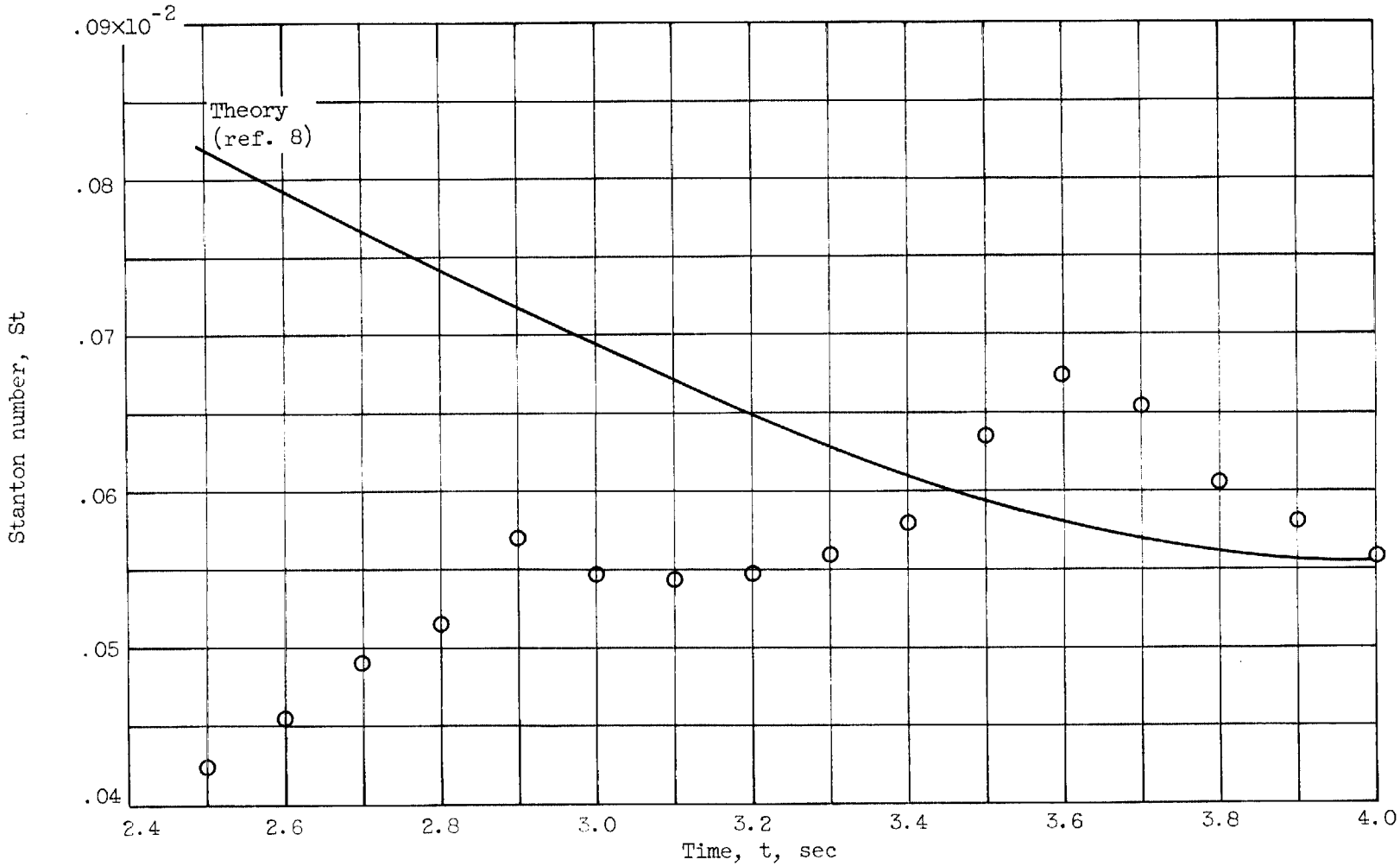

(b) Thermocouple station 9.

Figure 10. - Continued. Stanton number histories. Sharp tip conditions; cylinder stations.

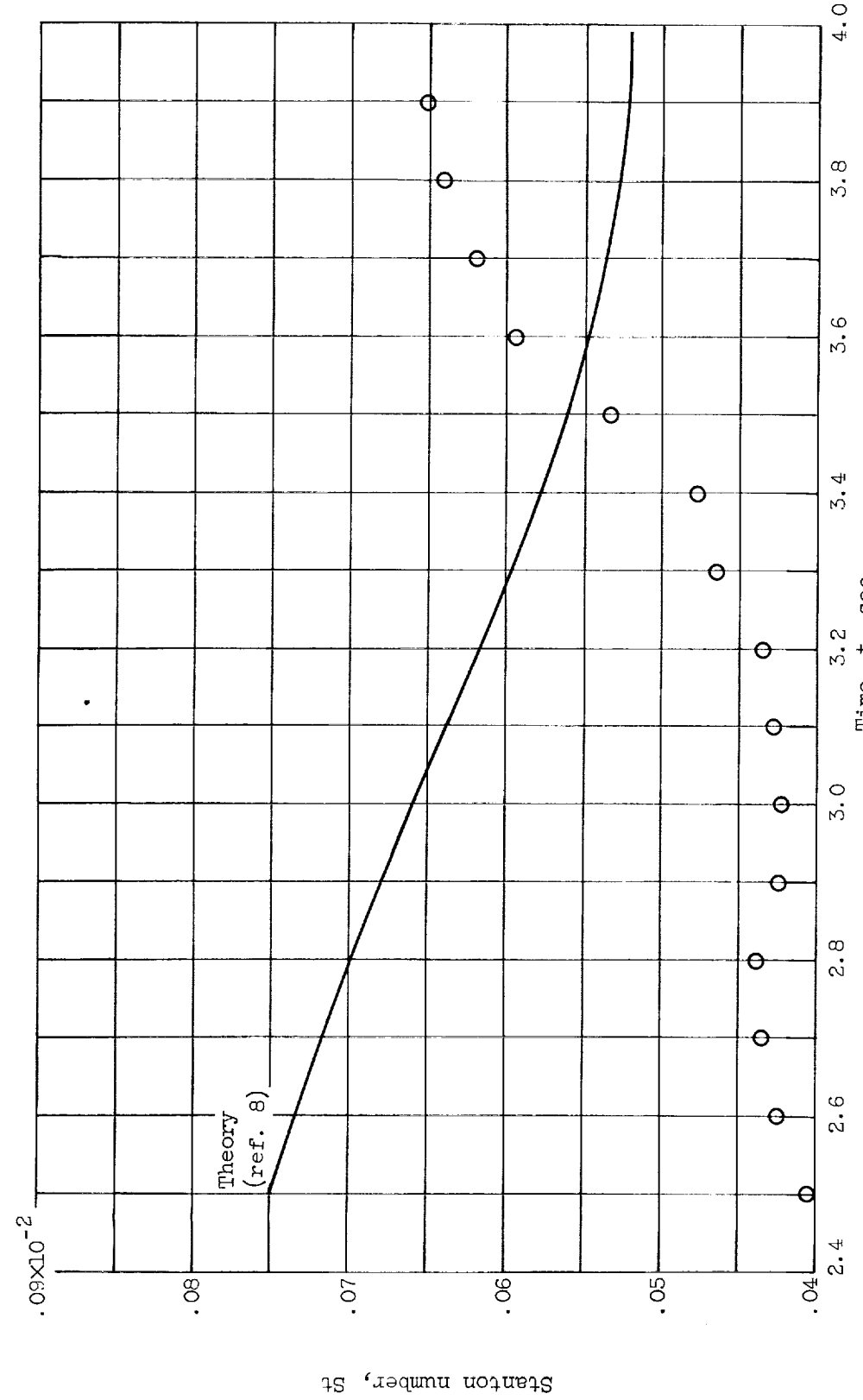

(c) Thermocouple station 10.

Figure 10. - Continued. Stanton number histories. Sharp tip conditions; cylinder stations.

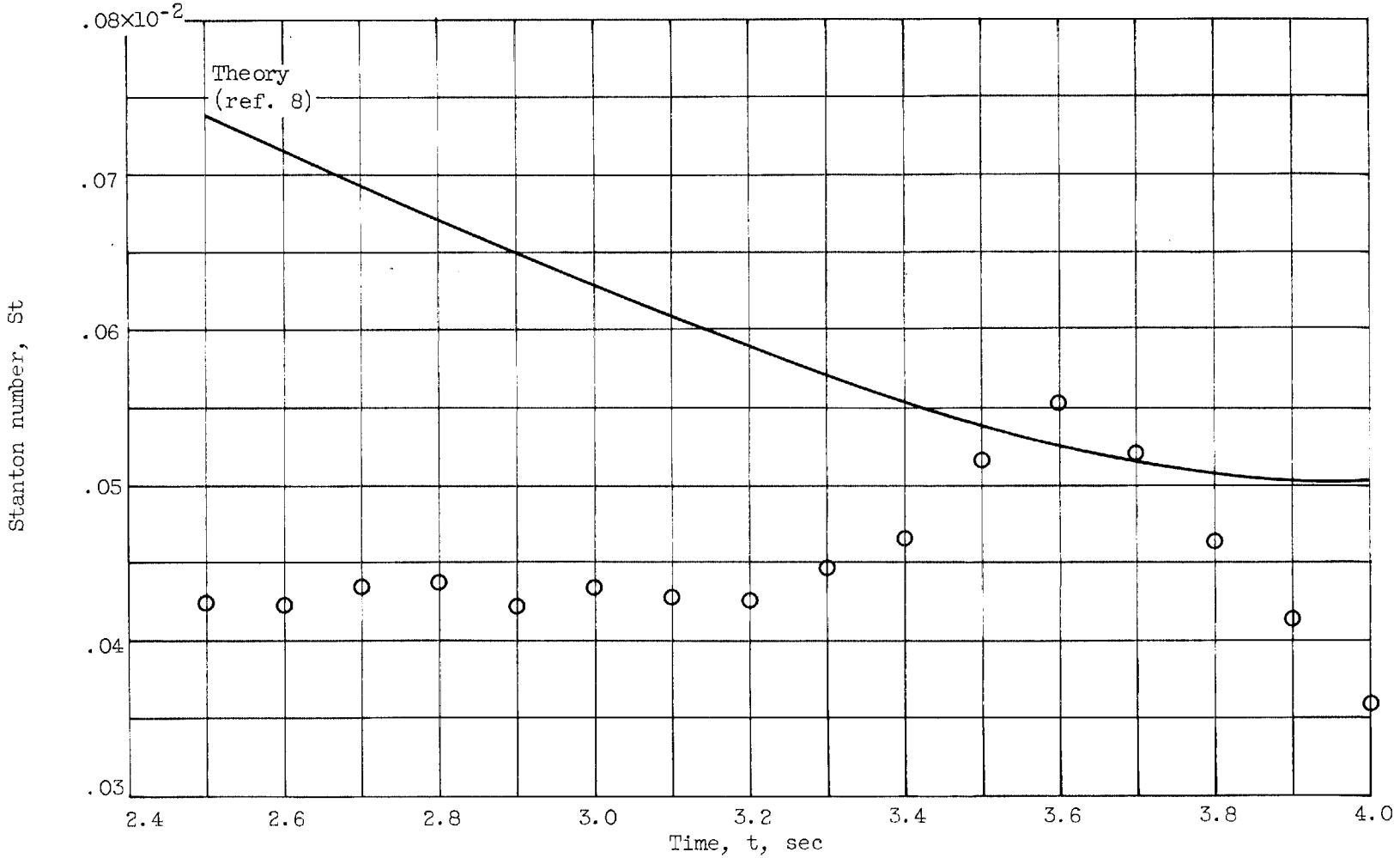

(d) Thermocouple station 11.

Figure 10. - Concluded. Stanton number histories. Sharp tip conditions; cylinder stations.

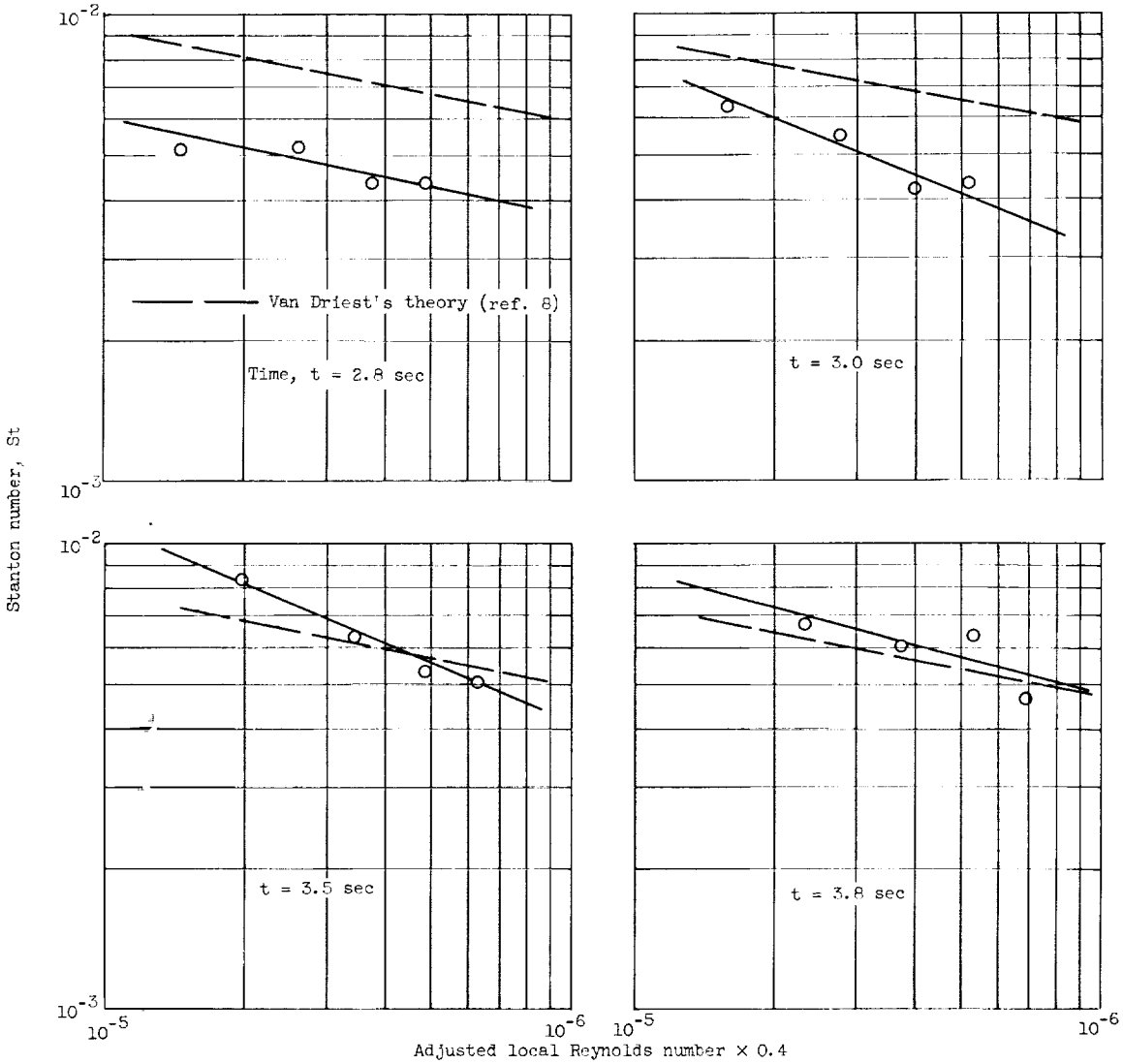

Figure 11. - Stanton number plotted against adjusted local Reynolds number. Sharp tip conditions; cylinder stations.

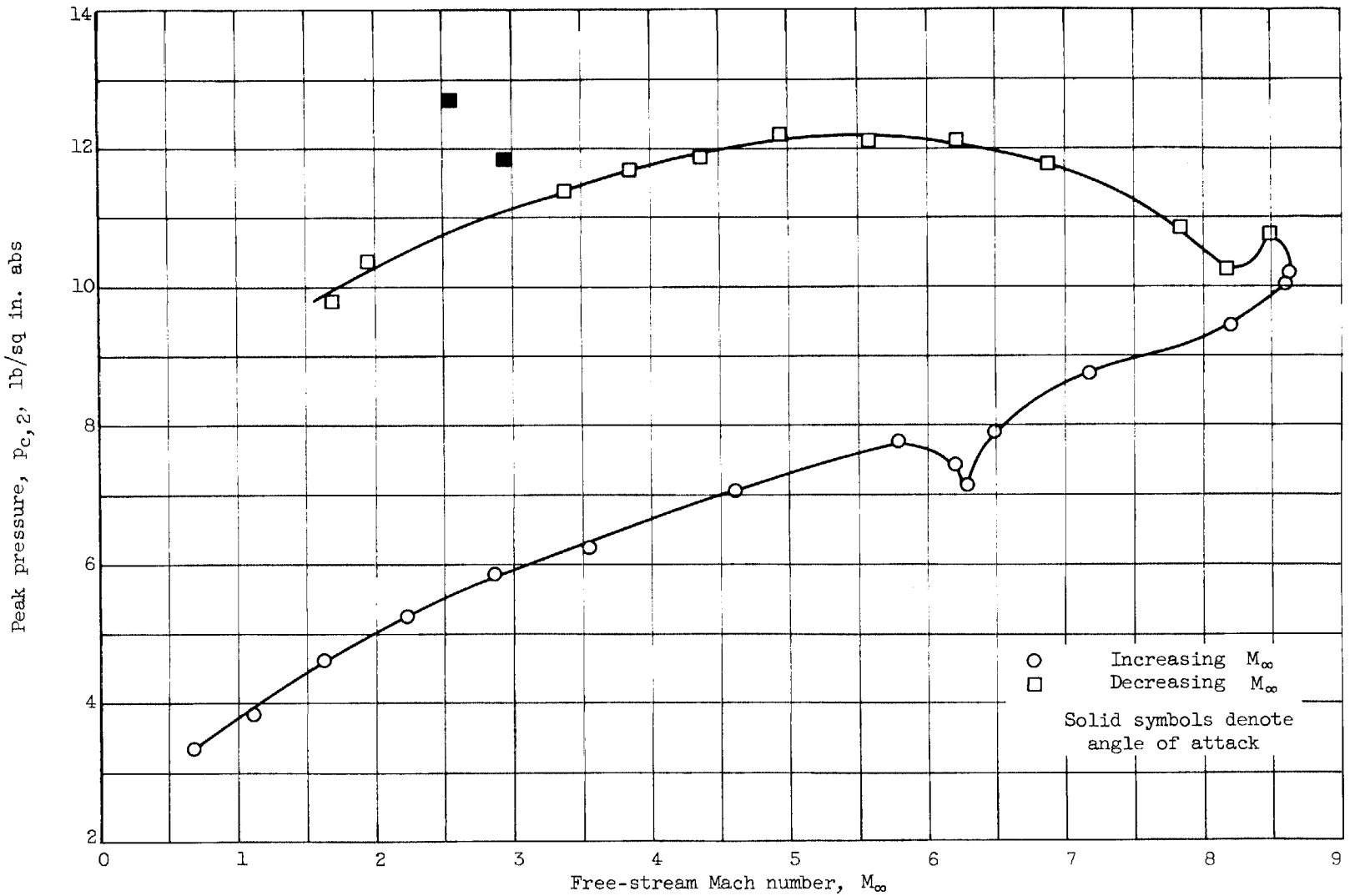

Figure 13. - Peak pressure - Mach number variation.

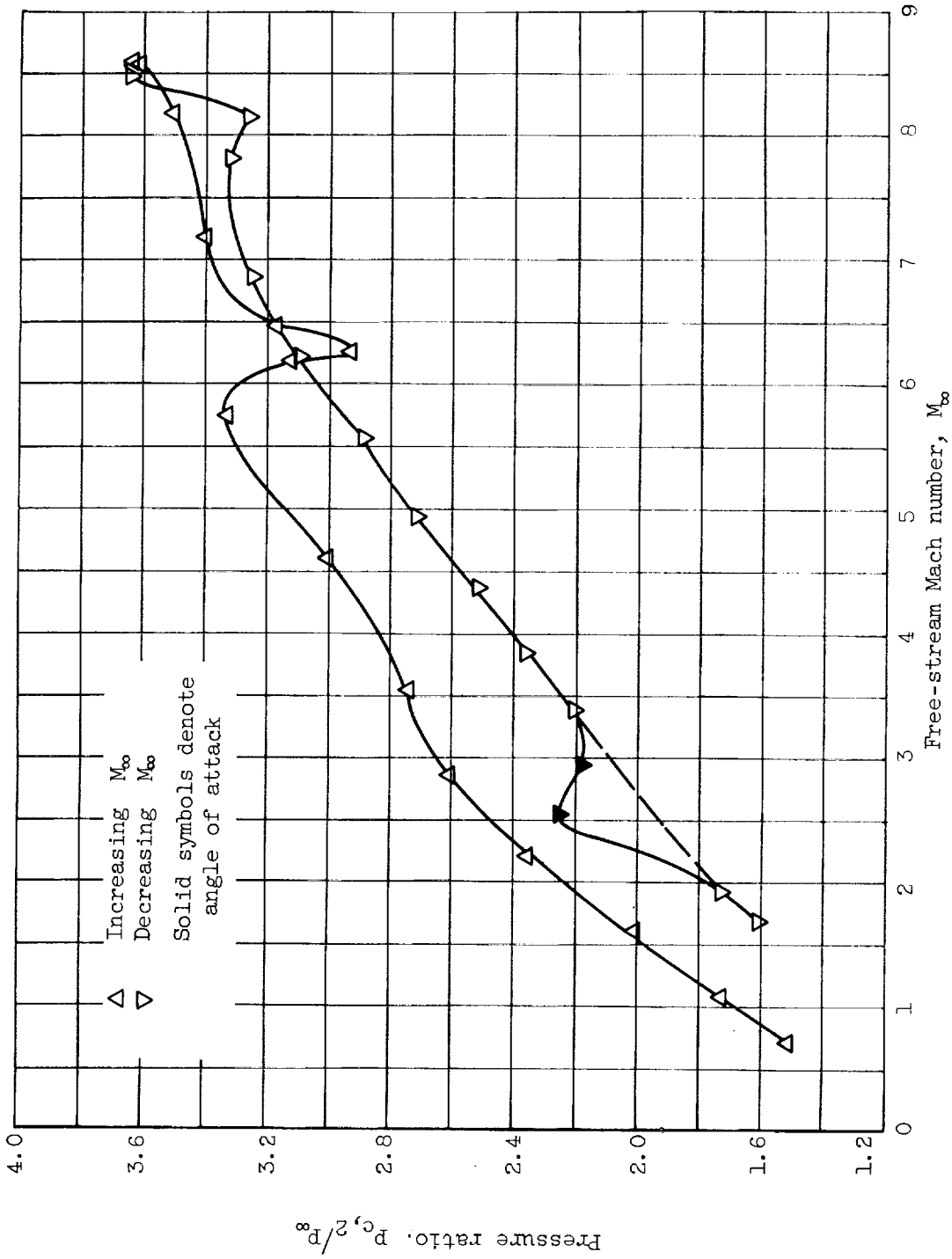

Figure 14. - Peak to free-stream pressure ratio variation with free-stream Mach number.

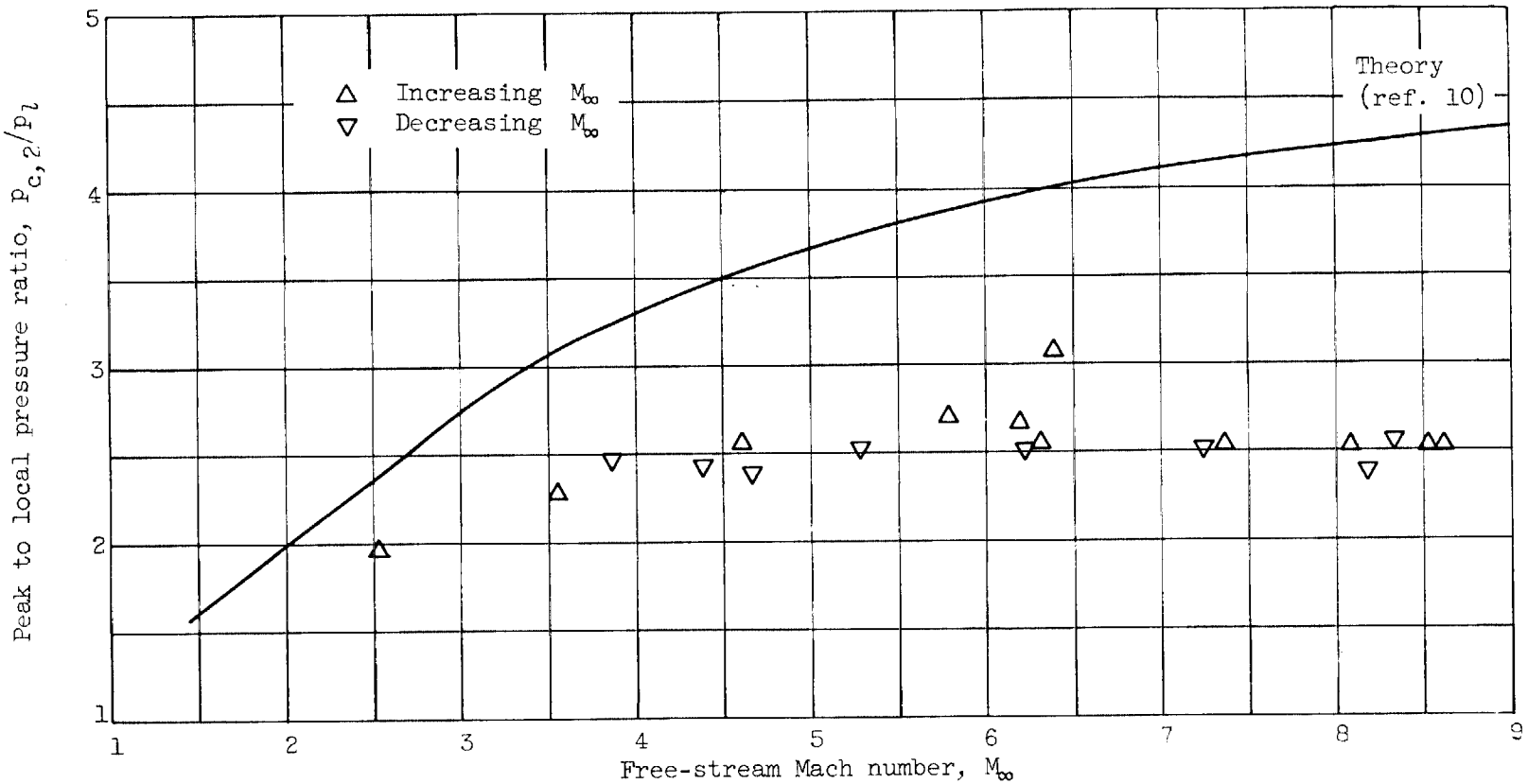

Figure 15. - Comparison of peak pressure ratios with theory.

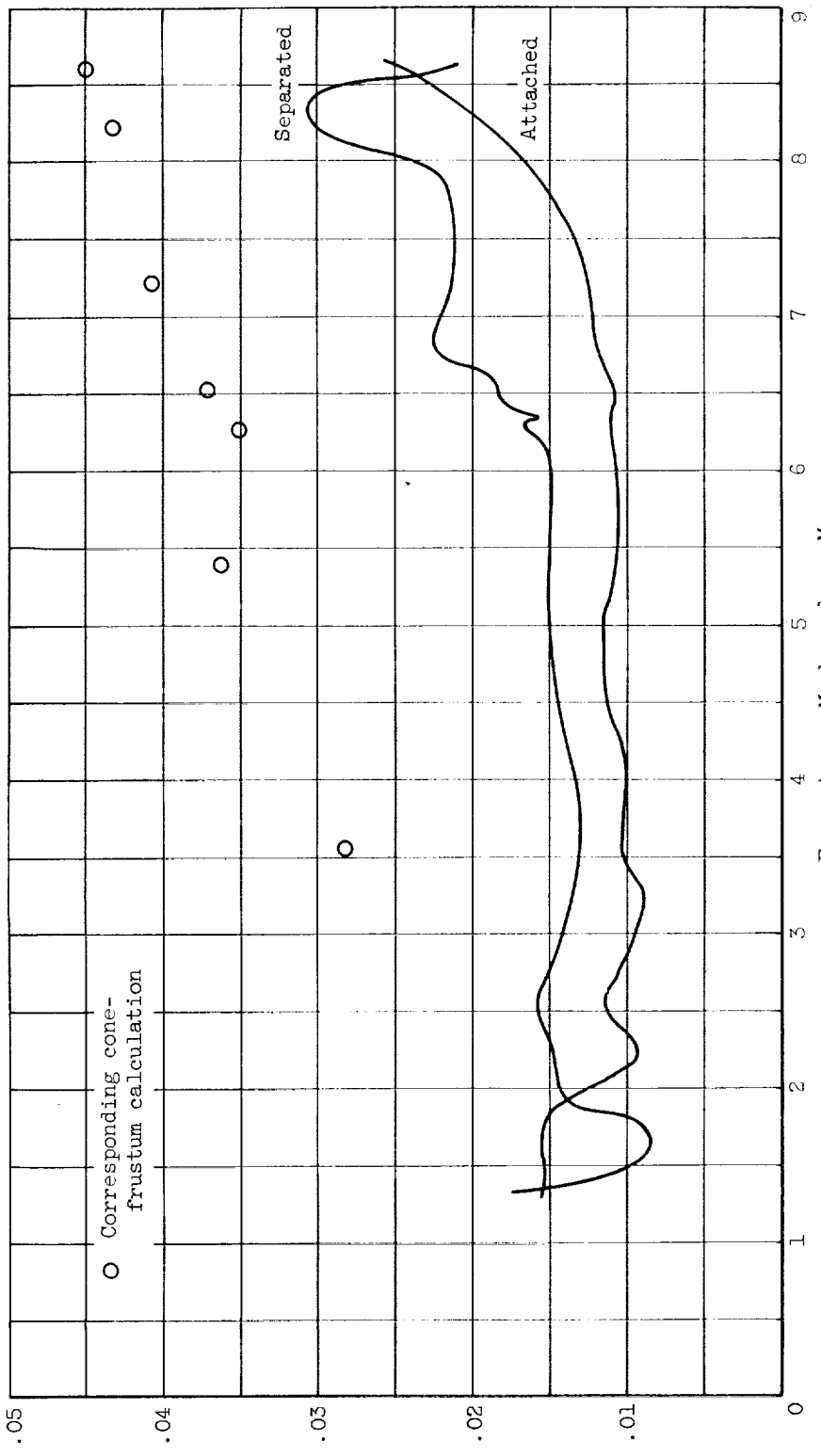

(a) Variation with flight Mach number.

Figure 16. - Measured heat-transfer coefficients in separated region.

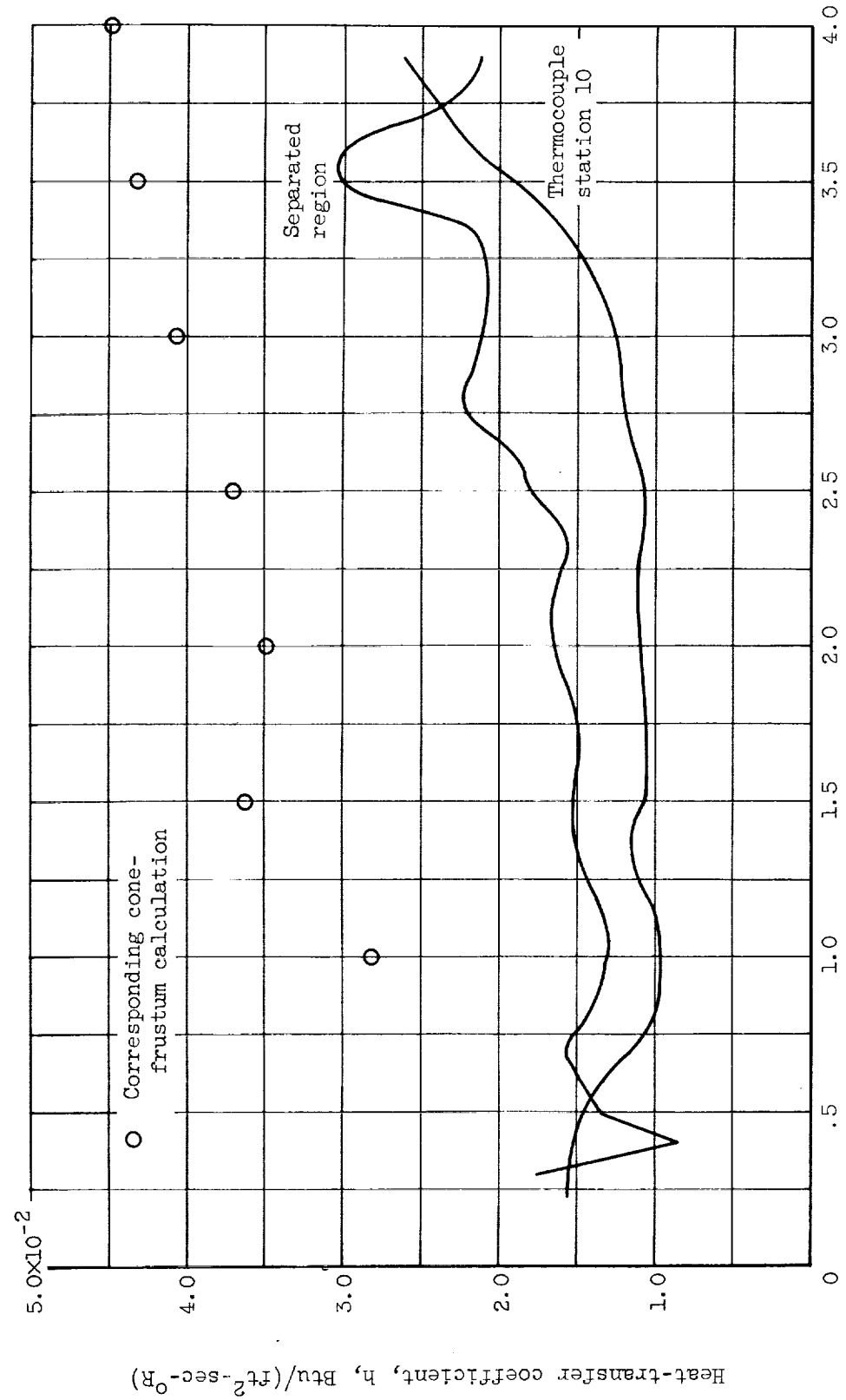

(b) Variation with time.

Figure 16. - Concluded. Measured heat-transfer coefficients in separated region.

E-545